Cell therapy with IL-10-producing group 2 innate lymphoid cells suppresses Graft-versus-Host disease

Kyle T. Reid[1,2], Sarah J. Colpitts[1,2], Jessica A. Mathews[2], Abel Santos Carreira[3], Julia M. Murphy[1,2], Dorota T. Borovsky[1], Wenhui Cui[1,2], Tommy Alfaro Moya[3,4], Nadia Sachewsky[2], James An[1,2], Yubing Xia[1,2], Arthur Mortha[1], Jong Bok Lee[2], Li Zhang[1,2,5], Igor Novitzky-Basso[1,3], Jonas Mattsson[1,3], and Sarah Q. Crome[1,2]

[1]Department of Immunology, Temerty Faculty of Medicine, University of Toronto, Toronto, Canada
[2]Toronto General Hospital Research Institute, Ajmera Transplant Centre, University Health Network, Toronto, Canada
[3]Princess Margaret Cancer Centre, University Health Network, Toronto, Canada
[4]Postgraduate Medical Education Program, Temerty Faculty of Medicine, University of Toronto, Toronto, Canada
[5]Department of Laboratory Medicine and Pathology, Temerty Faculty of Medicine, University of Toronto, Toronto, Canada

ORCID identifiers:
KTR: 0000-0003-4339-9317
SJC: 0000-0002-5657-8165
JAM: 0000-0003-2926-8222
JMM: 0000-0002-0617-1666
DTB: 0000-0002-6775-6641
TAM: 0000-0003-4171-4678
AM: 0000-0003-2673-0485
JBL: 0000-0002-4744-6021
LZ: 0000-0003-4649-0757
INB: 0000-0003-3748-3117
JM: 0000-0002-2163-6644
SQC: 0000-0001-5117-7453

***Correspondence:**
Sarah Q. Crome
email: sarah.crome@utoronto.ca
phone: 416.634.8097

Keywords: innate lymphoid cells, ILC2s, immune tolerance, immune regulation, cell therapy, graft-versus-host disease, hematopoietic stem cell transplant, graft-versus-leukemic effect

Short Title: $ILC2_{10}$ cell therapy inhibits GVHD

Number of Figures:7
Number of Supplemental Figures: 13

Abstract

IL-10 producing group 2 innate lymphoid cells ($ILC2_{10}$) have immunoregulatory functions, and limit harmful immune responses across various tissues. Despite their crucial roles in maintaining immune homeostasis, the cell therapy potential of human $ILC2_{10}$ has not been demonstrated, due to both limited numbers in human peripheral blood and lack of definitive markers for identification. Here, we isolate and expand circulating human $ILC2_{10}$, and assess their cell therapy potential in a humanized model of Graft-versus-Host Disease (GVHD). Cell therapy with human $ILC2_{10}$ decreased GVHD severity and prolonged survival of NOD-*scid* IL2Rγ^{null} (NSG) mice. Adoptive transfer of $ILC2_{10}$ inhibited pathogenic T cell proliferation and intestinal infiltration, and suppressed $CD4^+$ Th1 and $CD8^+$ Tc1 cells in an IL-4 and IL-10 dependent manner. Critically, increased proportions of ILC2s did not correlate with higher rates of cancer relapse in HSCT recipients, and adoptive transfer of $ILC2_{10}$ did not compromise graft-versus-leukemic (GVL) effects in a humanized model. Finally, we identify CD49d and CD86 as novel markers that discriminate $ILC2_{10}$ from conventional ILC2s. Collectively, these findings demonstrate the potential of harnessing $ILC2_{10}$ in cell therapies for GVHD and other immune-driven pathologies.

List of Abbreviations

ADT – Antibody derived tags
aGVHD – Acute Graft-Versus-Host Disease
AML – Acute myeloid leukemia
BMT – Bone marrow transplant
CBA – Cytometric Bead Array
CITE-Seq –Cellular Indexing of Transcriptomes and Epitopes by Sequencing
EOMES – Eomesodermin
FACS – Fluorescence Activated Cell Sorting
GVL – Graft-Versus-Leukemia Effect
HSCT – Hematopoietic Stem Cell Transplant
IHC – Immunohistochemistry
IL – Interleukin
ILCs – innate lymphoid cells
ILC1 – Group 1 innate lymphoid cells
ILC2 - Group 2 innate lymphoid cells
$ILC2_{10}$ – IL-10-producing ILC2s
ILC3 - Group 3 innate lymphoid cells
KIR – Killer Cell Immunoglobulin-like Receptors
LTi – Lymphoid Tissue Inducer Cells
MDSC – Myeloid derived suppressor cell
MSC – Mesenchymal stromal cell
NK Cells – Natural Killer cells
NSG – NOD-scid-IL2Rg^{null}
PMA – Phorbol 12-myristate 13-acetate
RT – Room Temperature
S.I. – Small Intestine
sLT – Surface Lymphotoxin
Tc1 – Cytotoxic T cell type 1
TGF-β – Transforming Growth Factor Beta
Th1 – T helper 1
Th17 – T helper 17
Tc1– Type 1 CD8+ cytotoxic T cell
Tr1 – Type 1 Regulatory T cell
Treg – Regulatory T cell
XenoGVHD – Xenogeneic Graft-versus-Host Disease

Introduction

Group 2 innate lymphoid cells (ILC2s) have important roles in orchestrating immune responses and controlling tissue homeostasis. Initially described as a homogeneous population defined by expression of CD127, CD161 and CRTh2 in humans, recent findings have made it clear that ILC2s can differ in phenotype and function, both between and within tissues(1–4). For example, environmental signals can promote inflammatory ILC2s such as those that underly harmful immune responses in allergy and asthma, or instead promote immunoregulatory ILC2s that limit harmful inflammation in diverse contexts(5–8). While human ILC2 heterogeneity has been widely described, we are only beginning to appreciate how these distinct ILC2 populations interface with other immune cells, as well as how these different populations can be inhibited or harnessed in immunotherapy approaches.

IL-10-producing group 2 innate lymphoid cells ($ILC2_{10}$) have been shown to inhibit immune responses in mouse models of inflammation and transplantation(9–14). For example, IL-2 administration induced IL-10 production in murine lung-resident ILC2s that have important functions in inhibiting and preventing lung inflammation (10), and intestinal mouse ILC2s were the primary producers of IL-10 at steady state and during disease(12). While there are few studies of human $ILC2_{10}$, they are significantly reduced in individuals with allergies, but expand in response to allergy immunotherapy and are associated with treatment response(13), supporting human $ILC2_{10}$ regulatory activity can be promoted with immunotherapy approaches to promote immune tolerance. The authors attempted to define unique $ILC2_{10}$ markers, reporting that KLRG1 marked ILC2s that produced IL-10 along with other signature ILC2 cytokines(13). However, KLRG1 has also been widely reported on ILC2s with pro-inflammatory functions, limiting the use of KLRG1 as a unique marker for $ILC2_{10}$(15–18). Therefore, identifying phenotypic features demarcating inflammatory and regulatory ILC2s is needed to enable comprehensive

analysis of these functionally distinct ILC2 populations to health and disease, and to perform in depth studies of $ILC2_{10}$ biology.

In addition to transplantation and autoimmunity, tolerogenic therapies are being widely pursued for the prevention and treatment of Graft-versus-Host Disease (GVHD) following allogeneic Hematopoietic Stem Cell Transplantation (HSCT). HSCT is a therapy commonly used to treat those with hematological malignancies, wherein transplanted donor stem cells develop into lymphocytes and attack cancerous cells, in what is termed the Graft-Versus-Leukemia(GVL) effect. While HSCT is often curative, up to 80% of patients develop acute GVHD characterized by donor T cells attacking healthy recipient tissues(19). Despite prophylactic use of post-transplant cyclophosphamide, acute GVHD remains the major cause of non-relapse associated morbidity and mortality, effecting 30-50% of HSCT recipients(20–24). Further, 30% of patients that develop GVHD fail to respond to corticosteroids or other broad immunosuppressive agents. Several regulatory cell therapy approaches have been explored in clinical trials, including adoptive transfer of regulatory T cells (Tregs). While evidence of Tregs limiting harmful allogeneic T cells have been reported, to date these cell therapies have only achieved limited clinical efficacy, and patients still require immunosuppression(25, 26). Therefore, there is an urgent need to develop more effective therapies for GVHD that do not impair GVL responses.

Prior studies reported ILCs are particularly sensitive to pre-HSCT conditioning therapies, where they are depleted from peripheral blood and tissues(27–29). Early Natural Killer (NK) cell reconstitution, in particular expansion of $CD56^{bright}$ NK cells(30, 31), or the presence of activated ILC2s and group 3 ILCs(ILC3s) are associated with reduced GVHD incidence(32). Intriguingly, Bruce *et al.* showed that adoptive transfer of mouse ILC2s improved intestinal barrier function via ILC2-derived amphiregulin (AREG), and transferred ILC2s recruited and activated myeloid derived suppressor cells (MDSCs) in an allogeneic bone marrow transplant model (27). Whether $ILC2_{10}$ specifically have protective functions in cell therapies for GVHD, and if $ILC2_{10}$ would have any direct effects on allogeneic T cell responses, has

not been explored. However, growing reports support ILC2$_{10}$ could be harnessed to promote immune tolerance (9–14).

Several challenges have prevented assessment of the cell therapy potential of human ILC2$_{10}$, the first and foremost being the relative paucity of human ILC2s in peripheral blood and lack of effective expansion protocols. To overcome this challenge, we developed methods to robustly expand ILC2$_{10}$ that display a stable phenotype. We then demonstrate cell therapy with ILC2$_{10}$ limits GVHD in a preclinical humanized mouse model, and that ILC2$_{10}$ do not impair GVL responses critical for HSCT therapeutic effectiveness. We define novel markers of expanded ILC2$_{10}$ that enable discrimination and isolation of ILC2$_{10}$ from conventional ILC2s. We also identify ILC2$_{10}$ directly suppress allogeneic T cell responses in a manner distinct from Tregs, as well as display distinct protective mechanism than what has been reported with conventional ILC2s. Findings herein provide proof-of-concept data to support cell therapy applications of human ILC2$_{10}$ for T cell-driven pathologies such as those that underlie GVHD.

Results

Expansion of human ILC2s with an ILC2$_{10}$ phenotype

Recent studies reporting protective functions of ILC2s and ILC2$_{10}$ in multiple contexts supported that targeting or harnessing ILC2s in immunotherapy approaches may have benefits in dampening harmful inflammation. To explore this possibility, we first had to develop methods to isolate and expand large numbers of human ILC2s. ILC2s are present in very low abundance in peripheral blood and tissues, and most expansion protocols from mouse rely on *in vivo* cytokine administration prior to isolating ILC2s from bone marrow or other tissues, which would not be compatible with cell therapy approaches. Here,

we isolated human ILC2s, as well as NK cells and ILC3s for comparison, from normal donor peripheral blood mononuclear cells (PBMCs) by flow cytometry sorting using a combination of ILC markers and gating out lineage positive cells (**Supplemental Figure.1A, B**). $CD56^{dim}$ NK cells were sorted as live $lineage^{-}CD45^{+}CD56^{+}CD16^{+}$, ILC2s as live $lineage^{-}CD45^{+}CD94^{-}CD16^{-}NKG2D^{-}CD127^{+}CRTh2^{+}CCR6^{-}$ and ILC3s as live $lineage^{-}CD45^{+}CD94^{-}CD16^{-}NKG2D^{-}CD127^{+}CRTh2^{-}CD117^{+}CCR6^{+}$. NK cells were expanded in NK MACS media supplemented with IL-2, IL-15 and IL-18, ILC2s were then expanded in X-VIVO media supplemented with IL-2, IL-7 and IL-33, and ILC3s were expanded in X-VIVO media with IL-1β, IL-2, IL-7 and IL-23. ILC2s and ILC3s exhibited robust expansion using this protocol, resulting in an average of $2.3x10^4 \pm 7.2x10^3$ and $9.8x10^3 \pm 3.6x10^3$ fold expansion respectively after 34 days in culture(**Supplemental Figure.1C**). Post-expansion, ILC2s strongly co-expressed IL-4, IL-13, IL-9 and GM-CSF following PMA-ionomycin stimulation, with low to no expression of IFN-γ, IL-17A or IL-22(**Figure.1A,B, Supplemental Figure.1D**). In contrast, expanded $CD56^{dim}$ NK cells co-expressed IFN-γ and TNF-α and ILC3s expressed IL-22 and GM-CSF, with low IL-17A expression(**Figure.1A,B, Supplemental Figure.1D,2A**). Secreted cytokine production in expanded ILCs was quantified using cytometric bead array(CBA) following stimulation with IL-2. ILC2s secreted high amounts of IL-4, IL-9, IL-5 and IL-13, whereas NK cells and ILC3s did not produce significant amounts of these cytokines and instead produced canonical cytokines including IFN-γ and TNF-α or IL-22, respectively(**Figure.1C**, **Supplemental Figure.2B**). In addition to cytokine expression, we also examined chemokine production. Expanded ILC2s also produced the chemokines CCL2, CCL11, CCL20 and CXCL10 (**Supplemental Figure.2D**). To confirm ILC2 stability, we assessed the phenotype of expanded ILC2s when cultured in ILC3 or NK cell medium for 10 days(**Supplemental Figure.3A-J**). Expanded ILC2s maintained expression of signature cytokines and did not upregulate cytokines associated with NK cells or ILC3s, supporting once activated and expanded, human ILC2s from healthy donor blood maintained a stable ILC2 phenotype.

194 To confirm expanded ILC2s maintained an ILC2-associated gene and protein expression profile, as well
195 as enable detailed phenotyping of expanded ILC2s, we preformed Cellular Indexing of Transcriptomes
196 and Epitopes by Sequencing(CITE-seq) on expanded ILCs. Expanded ILCs were stained with a
197 TotalSeq-C antibody cocktail and labelled with hashtag antibodies to enable easy identification after
198 sequencing(**Figure.1D, Supplemental Table 1**). All ILCs examined expressed lineage defining markers
199 that differentiated them from other family members. $CD56^{bright}$ and $CD56^{dim}$ NK cells expressed *GNLY*
200 and CD56, while the $CD56^{dim}$ NK cells expressed CD16. ILC3s strongly expressed CD117 and ILC2s
201 expressed *PTGDR2, GATA3, IL17RB, IL13* and *IL5* (**Figure.1E**). Intriguingly, one of the top genes
202 identified as being uniquely expressed by *ex vivo* expanded ILC2s was *IL-10* (**Figure.1E**), which we
203 validated by flow cytometry and cytometric bead array(**Figure.1F,G**). Expanded ILC2 supernatants had
204 consistently high levels of IL-10 secretion across all donors, and a high proportion of $IL\text{-}10^{+}$ cells were
205 noted in the majority of donors examined(**Figure.1F,G**). Therefore, ILC2s isolated and expanded using
206 our approach had a phenotype consistent with being $ILC2_{10}$.

207 Due to recent studies that identified murine $ILC2_{10}$ as having immunoregulatory properties, including
208 being able to suppress T cells(10, 13, 33), we assessed expanded ILC2s with $ILC2_{10}$ phenotype for
209 potential immunoregulatory properties beyond IL-10 production, or expression markers that overlapped
210 with other regulatory populations such as regulatory $CD4^{+}FOXP3^{+}$ Tregs and T regulatory 1 (Tr1) cells.
211 Low or background expression of checkpoint molecules such as PD-1, PD-L1, CTLA-4, LAG3 was
212 observed at both the RNA and protein level, and no *FOXP3* gene transcript was observed**(Supplemental**
213 **Figure.4A,B)**(34, 35). Additionally, we did not detect *IL12A* and *EBI3*, which make up the regulatory
214 cytokine IL-35**(Supplemental Figure.4A,B)**. Despite ubiquitous transcriptional expression of *TGFB1*
215 across ILC subsets, no protein-level expression of active TGF-β1 was observed in expanded NK cells,
216 ILC2s or ILC3s(**Supplemental Figure.2C, Supplemental Figure.4B**). While these regulatory molecules
217 were absent, expanded ILC2s expressed *ENTPD1*, the gene for CD39(**Supplemental Figure.4C**) and

also weakly expressed *NT5E* (CD73). However only ILC2s and CD56^{bright} NK cells exhibited surface CD73 protein expression(**Supplemental Figure.4C**). Flow cytometry analysis verified expanded ILC2s co-expressing high levels of CD73, in line with reports of *ex vivo* ILC2s(36) as well as CD39(**Supplemental Figure.4D,E**), which are known to inhibit the functional activity of T cells(37, 38). IL-10 expression on ILC2s was correlated with co-expression of IL-4, as well as amphiregulin (AREG) but had no significant correlation to expression levels IL-9 or IL-13 cytokines(**Figure1.H-K**). High amphiregulin was also notable, as it is a key tissue reparative effects(27, 39, 40), and was linked to ILC2s protective effects in limiting GVHD, supporting dual regulatory and reparative potential of expaned $ILC2_{10}$.

Adoptive transfer of allogeneic human $ILC2_{10}$ suppresses xenogeneic GVHD

Pre-clinical models and patient-based studies have linked $CD4^+$ T helper 1(Th1) and $CD8^+$ cytotoxic T cells (Tc1) to aGVHD pathology(41–44). 30% of aGVHD patients do not respond to first line corticosteroid treatment, with less than one-third of non-responders surviving past one year(45), highlighting the need to identify cells and molecules that limit pathogenic T cell responses post-HSCT. Due to prior mouse studies supporting potential applications of ILC2 transfer for GVHD(27, 46), and increasing appreciation of immunoregulatory functions of $ILC2_{10}$, we sought to assess the cell therapy potential of human $ILC2_{10}$ using a preclinical xenogeneic GVHD model(xenoGVHD). In this model, 6–8-week-old female NOD-scid-IL2Rg^{null} (NSG) mice are irradiated and injected with human PBMCs. T cells from transferred PBMCs engraft into NSG mice and induce tissue pathology similar to acute GVHD (47). NSG mice are monitored for signs of xenoGVHD, using weight-loss and a composite xenoGVHD score, which measures fur loss, skin inflammation, hunch, activity, and pain (**Figure.2A**). T cell

engraftment, as well as detailed phenotyping is performed on circulating immune cells and immune cells within tissues at endpoint or indicated times.

Using this model, we assessed whether cell therapy with $ILC2_{10}$ could limit human T cell-mediated pathology. NSG mice that received PBMCs alone or PBMCs and $ILC2_{10}$ were first compared for signs of GVHD and how this corresponded with T cell engraftment. After 14 days, engraftment of human $CD45^+CD3^+$T cells was observed in the blood, with no significant difference in T cell proportions between NSG mice given human PBMCs alone or mice treated with $ILC2_{10}$, indicating $ILC2_{10}$ did not inhibit T cell engraftment(**Figure.2B-D**). This was of note, as cell therapy with Tregs in this xenoGVHD model results in impaired T cell engraftment (48). Despite not impacting T cell engraftment, female NSG mice treated with $ILC2_{10}$ had significantly delayed onset and reduced GVHD symptoms, including decreased weight-loss across 3 independent experiments (**Figure.2E-H**). These effects were also observed in separate experiments in male NSG mice, although with slight differences in xenoGVHD kinetics(**Supplemental Figure.5A-C**). This single infusion of $ILC2_{10}$ not only reduced xenoGVHD severity but also significantly improved overall survival(**Figure.2I**). Notably $ILC2_{10}$-treated mice only reached endpoint due to weight-loss, but other GVHD symptoms were still very low and mice would otherwise not have reached endpoint(**Figure.2E,F**).

To assess if $ILC2_{10}$ could also treat GVHD upon onset, allogeneic $ILC2_{10}$ were adoptively transferred after T cell engraftment and onset of xenoGVHD symptoms. Here, T cell engraftment was confirmed prior to $ILC2_{10}$ transfer, and mice had begun displaying early xenoGVHD symptoms. When human $ILC2_{10}$ were transferred at day 9, this resulted in similar protection from xenoGVHD to when $ILC2_{10}$ were administered prophylactically at day 0(**Supplemental Figure 6)**. Taken together, cell therapy with allogeneic expanded human $ILC2_{10}$ limited pathology and enhanced overall survival in this model of GVHD when administered both prophylactically and upon GVHD onset.

$ILC2_{10}$ inhibit allogeneic T cell responses in xenoGVHD

We next sought to determine how $ILC2_{10}$ protected from GVHD. Similar to previous reports, T cells made up >96% of engrafted human $CD45^+$cells across all organs analyzed (**Figure 2B-D** and **Supplemental Figure.7A-D)**(47). Despite no differences in engraftment at day 14, we noted at endpoint a moderate increase in $CD4^+$ Th cells and reciprocal decrease in cytotoxic $CD8^+$ T cells in the blood, bone marrow and spleen of NSG mice receiving $ILC2_{10}$ cell therapy(**Figure.2J**). We observed $CD4^+$ and $CD8^+$ T cells had reduced expression of Ki-67 in the blood, bone marrow and spleen of NSG mice treated with $ILC2_{10}$, indicating reduced T cell proliferation (**Figure.3A-D**, **Supplemental Figure.8A,B).** This was not accompanied by changes in T cell expression of checkpoint molecules examined including PD-1, CTLA-4 and CD25 (**Supplemental Figure.9A-C**).

Previous research has indicated that $CXCR3^+$T cells drive trafficking to target organs including intestines in mouse models of GVHD(49, 50). CXCR3 also marks $CD4^+$ Th1 and $CD8^+$ Tc1 cells(51–53) which induce intestinal damage in GVHD models and correlate with disease in patients(41, 43). We therefore asked whether $ILC2_{10}$ influenced T cell phenotypes and intestinal trafficking within the xenoGVHD model. CD3 immunohistochemical(IHC) staining of tissues revealed a stark reduction in T cell infiltration into colons of $ILC2_{10}$-treated mice, with no change in T cell infiltration noted in the lungs, spleen, or liver(**Figure.3E,F**, **Supplemental Figure.10A-G**). Across compartments examined, mice receiving $ILC2_{10}$ cell therapy had reduced CXCR3 expression by $CD4^+$ and $CD8^+$ T cells(**Figure.3G-J**, **Supplemental Figure.8C,D**), with no increase in CRTh2 or CCR6, markers of $CD4^+$ T helper 2 (Th2) and T helper 17 (Th17) cells, respectively(52–54). Adoptive transfer of human $ILC2_{10}$ therefore did not promote differentiation to other T cell subsets, but inhibited $CD4^+$Th1 and $CD8^+$Tc1 cells(**Figure.3G-J, Supplemental Figure.8C,D**)(52–54).

286

287 **Inverse correlation between ILC2s and pathogenic T cells in HSCT recipients**

288 Due to ILC2$_{10}$-mediated suppression of CD4$^+$ Th1 and CD8$^+$ Tc1 cells in the xenoGVHD model, and
289 prior studies reported increased CD56^{bright} NK cells, ILC2s and ILC3s in peripheral blood of HSCT
290 patients that did not develop GVHD compared to those that did(32), we were interested in the
291 relationships between ILCs and T cell subsets in HSCT recipients with differing clinical outcomes. We
292 analyzed the proportion of subsets of ILCs and T cells in the blood of HSCT patients at the time of
293 aGVHD diagnosis and compared proportions of these populations in patients without aGVHD and
294 healthy donors(**Supplemental Figure.11A**, **Supplemental Table 2**). All HSCT recipients were given
295 prophylactic post-transplant cyclophosphamide, and two were treated with additional
296 immunosuppression at the time of sample acquisition. In line with previous literature, patients without
297 aGVHD had decreased proportions of CD56^{dim} NK cells and increased proportions of CD56^{bright} NK
298 cells(30, 31)(**Supplemental Figure.11B,C**). Similarly, patients that developed aGVHD had a reduced
299 proportion of total helper ILCs (Lin$^-$ CD127$^+$)(**Figure.4A,B**), with reduced proportions of ILC1s, ILC2s
300 and ILC3s compared to healthy controls(**Figure.4C,D).** HSCT patients without aGVHD, however, had
301 significantly higher proportions of ILC2s, but no significant differences in ILC1s or ILC3s compared to
302 patients with aGVHD with our sample size (**Figure.4C,D**).

303 We next examined the correlation of ILCs with T cell subsets in HSCT recipient peripheral blood.
304 Similar to what we observed with ILC2 therapy in the xenoGVHD model, HSCT recipients with aGVHD
305 had increased CD4$^+$ Th1 and CD8$^+$ Tc1 cells as a proportion of total CD4$^+$ and CD8$^+$ T cells
306 respectively(**Figure.4E,F**), with no significant difference in circulating Th17 cells (51–53). Elevated
307 ILC2s, significantly correlated with low proportions of Th1 cells as a percent of CD3$^+$ T across all HSCT
308 patients(**Figure.4G-H**). Therefore, ILC2s proportions following HSCT are associated with decreased

pathogenic T cell responses, mirroring findings in our xenoGVHD model, and further supporting the therapeutic potential of ILC2s for GVHD. While this paralleled the inverse relationship observed in xenoGVHD model, a caveat was that we were not able to specifically examine whether these ILC2s were specifically $ILC2_{10}$, as markers of $IL10^{+}ILC2$s had not been established.

Expanded IL-10^{+}ILC2s regulate $CD4^{+}$ and $CD8^{+}$ T cells via IL-4 and IL-10

We next asked whether $ILC2_{10}$ could directly regulate allogeneic T cells. *In vitro* co-cultures were performed with $ILC2_{10}$ and allogeneic naïve $CD4^{+}$ or $CD8^{+}$ T cells. Culture with $ILC2_{10}$ resulted in a significant reduction in IFN-γ^{+} and IFN-γ^{+}/TNF-α^{+} $CD4^{+}$ T cells(**Figure.5A,B**). Decreased IFN-γ was also observed when allogeneic $ILC2_{10}$ were cultured with $CD8^{+}$ T cells(**Figure.5C,D**). To confirm *in vivo* findings that cell therapy with $ILC2_{10}$ reduced Th1 and Tc1 cells without increasing proportions of Th2 or Th17 cells, we also examined cytokines expressed by other T cell subsets. No increase in IL-17A, IL-22, IL-4, IL-9 or IL-13 was observed with addition of $ILC2_{10}$ to cultures with $CD4^{+}$ or $CD8^{+}$ T cells(**Supplemental Figure.12A,B**). Thus, decreased IFN-γ does not appear to be due to T cell differentiation into other T cell subsets, but $ILC2_{10}$-mediated inhibition of $CD4^{+}$ Th1 and $CD8^{+}$Tc1 cells.

We next explored whether various molecules associated with ILC2s or $ILC2_{10}$ identified by CITE-seq controlled ILC2-mediated regulation of T cells interactions. We noted that allogeneic T cells activated in the presence of supernatants from IL-2-stimulated $ILC2_{10}$ had comparable suppression of T cells to that of adding ILC2s to T cell cultures directly(**Supplemental Figure.12C,D**), indicating one or more secreted factors produced by $ILC2_{10}$ underlies their ability to inhibit T cells.

329 $ILC2_{10}$ were therefore cultured with allogeneic T cells in the presence or absence of neutralizing
330 antibodies or inhibitors to secreted molecules of interest(IL-10, CD39, CD73), as well as ILC2 cytokines
331 (IL-4, IL-9, IL-13)(6, 55, 56). The addition of an IL-4-neutralizing antibody strongly reduced $ILC2_{10}$-
332 mediated suppression of IFN-γ by $CD4^+$ T cells *in vitro,* but blocking IL-9, IL-13 or CD39/CD73 had no
333 effect(**Figure.5E,F**, **Supplemental Figure.12E, Supplemental Figure.13A**). Neutralizing IL-10 also
334 decreased suppression of $CD4^+$ T cell-IFN-γ, but to a lesser extent than IL-4(**Figure.5E,F,**
335 **Supplemental Figure.13A**). In contrast, the combination of anti-IL-4 and anti-IL-10 abrogated $ILC2_{10}$-
336 mediated suppression of IFN-γ by $CD8^+$ T cells, which was not observed with anti-IL-4 or anti-IL-10
337 alone(**Figure.5E,G, Supplemental Figure.13B**). $ILC2_{10}$ suppression of allogeneic $CD4^+$ and $CD8^+$ T
338 cells cytokine production requires IL-4 and IL-10, with differing contributions of IL-4 and IL-10 to the
339 regulation of $CD8^+$ and $CD4^+$ T cells.

340

341 **Allogeneic human $ILC2_{10}$ do not suppress T cell mediated graft-versus-leukemia effects**

342 The GVL effect is critical for success of allogeneic HSCT for treating hematological malignancies.
343 While cell therapy with $ILC2_{10}$ did not impair T cell engraftment, $ILC2_{10}$ suppressed xenogeneic T cell
344 responses. A key question therefore was whether cell therapy with $ILC2_{10}$ would inhibit T cell-mediated
345 GVL effects. Within our clinical cohort, we assessed circulating ILC2 proportions and how they
346 correlated with relapse status. No significant differences in ILC2 proportions was observed in the blood
347 of patients which went on to experience relapse of their malignancy, supporting that increased
348 proportions of ILC2s are not associated with reduced GVL effects(**Figure.6A**).

349 We next assessed whether $ILC2_{10}$ cell therapy would negatively impact T cell-mediated GVL-effects in a
350 in a humanized mouse model. Briefly, MV4-11 cells, an acute myeloid leukemia cell line, were injected

into mice 5 days prior to transfer of PBMCs alone or PBMCs with allogeneic expanded human $ILC2_{10}$ (**Figure.6B**). The ability of T cells to kill MV4-11 cells was then assessed at day 14 following PBMC transfer. As expected, PBMC injection resulted in a reduction in MV4-11 cells in the bone marrow compared to mice receiving MV4-11 cells alone(**Figure.6C,D)**. Mice treated allogeneic $ILC2_{10}$ had comparable reductions in MV4-11 cells within the bone marrow to that observed with mice receiving PBMCs alone(**Figure.6C,D**), supporting $ILC2_{10}$ were not impeding T cell-mediated GVL responses. Importantly, within the same mice, $ILC2_{10}$ treatment reduced xenoGVHD symptoms similar to what was observed without MV4-11 transfer(**Figure.6E**), clearly showing simultaneous protection from pathogenic T cell responses that underlie GVHD without impairing T cell-mediated GVL effects. Collectively our findings support $ILC2_{10}$ do not limit the anti-leukemic effect of allogeneic T cells despite protecting from GVHD, therefore representing a strong candidate for cell-based therapies for GVHD following HSCT.

Ex vivo expanded $ILC2_{10}$ highly express CD49d and CD86

Despite consistently high levels of IL-10 in our *ex vivo* expanded $ILC2_{10}$, we noted heterogeneity in the proportions of IL-10^+ cells between ILC2 isolations from different donors. In order to improve consistency of $ILC2_{10}$ in cell expansions, as well as define key molecules that differentiate IL-10^+ILC2s from IL10^-ILC2s, we performed differential gene expression analysis of *IL10*$^+$ILC2s to *IL10*$^-$ILC2s in our CITEseq dataset on expanded human ILCs. Elevated expression of CD86 and *ITGA4* (CD49d) was noted on the *IL10*$^+$ILC2s(**Figure.7A**), which was confirmed by flow cytometry to identify IL-10^+ILC2s (**Figure.7B,C**). We also examined CD117 expression, as *ex vivo* ILC2s had variable expression of CD117 during isolation, and KLRG1, which was previously reported to be expressed by IL-10-producing ILC2(13). Both IL-10^+ and IL-10^-ILC2s had very low expression of these molecules, although we noted a

small but significant fold increase in CD117 expression(**Figure.7D,E**). Using tSNE clustering following flow cytometry staining, a distinct cluster expressing IL-10 was defined by high expression of CD49d and CD86 (**Figure.7F**). Dividing expanded ILC2s into populations based on expression of CD49d, CD86 or co-expression revealed CD49d and CD86 marked IL10-expressing ILC2s with the highest IL-10 expression on $CD49d^{+}CD86^{+}$ ILC2s(**Figure.7F**). CD49d and CD86 expression therefore identify *ex vivo* expanded $ILC2_{10}$, and can be used to isolate $ILC2_{10}$ in expansion cultures.

To assess the potential utility of these markers to identify $ILC2_{10}$ in patient-based studies, we examined the publicly available scRNA-seq dataset of ILCs from patients with grass-pollen allergy treated with either grass-pollen sublingual allergen-specific immunotherapy(GP-SLIT) or placebo (PL-SLIT)(13). Here, the authors reported that patients treated with GP-SLIT had improved outcomes and increased proportions of $ILC2_{10}$ at 12-month and 24-month follow-ups compared to placebo treated patients. Further, the authors reported KLRG1 expression defined $ILC2_{10}$, and pathways related to IL-10 signalling and regulation were upregulated in at both time points following GP-SLIT. We re-analyzed this scRNA-seq dataset to evaluate whether the increased IL-10 expression by ILC2s was associated with increases in CD49d and CD86. Following clustering of ILC2s from GP-SLIT treated patients, there was increased expression of *IL10* as reported, as well as *IL4* (**Figure.7G)**. Further, GP-SLIT treated patients had elevated expression of *IL2RA, IL7R* and *IL1RL1,* receptors for the cytokines used for our $ILC2_{10}$ expansion (**Figure.7G)**. Notably, ILC2s from GP-SLIT treated patients had elevated expression of *ITGA4* (CD49d) and *CD86,* in addition to elevated *KLRG1* expression as reported (**Figure.7G**). This elevated expression of CD49d and CD86 that correlated with $ILC2_{10}$ supports the potential broad applications of these markers to differentiate $ILC2_{10}$ from inflammatory ILC2s in human studies.

Discussion

This proof-of-concept study demonstrates the cell therapy potential of human $ILC2_{10}$, and their capacity to directly regulate harmful T cell responses that drive GVHD pathology. $ILC2_{10}$ were robustly expanded using our approach, and displayed a stable phenotype. Importantly, $ILC2_{10}$ cell therapy inhibited development of GVHD in humanized mouse models without impairing GVL effects essential for the success of HSCT. These findings mirror HSCT patient-based studies, where high ILC2 proportions are associated with protection from GVHD, without increased risk of cancer relapse. Human $CD4^+$ and $CD8^+$ T cells had reduced proliferation, tissue trafficking, and intestinal infiltration following $ILC2_{10}$ treatment, and there were decreased proportions of $CD4^+$Th1 and $CD8^+$Tc1 cells across multiple tissue sites with $ILC2_{10}$ therapy. Direct regulation of allogeneic T cell responses in this manner is unique to $ILC2_{10}$ cell therapy, as it was not reported in mouse studies of conventional ILC2s, or in Treg studies using this xenogeneic GVHD model (27). CD86 and CD49d marked *ex vivo* expanded $ILC2_{10}$, which suppressed IFN-γ in $CD4^+$ and $CD8^+$ T cells through a combination of IL-10 and IL-4. Altogether, our findings support that human $ILC2_{10}$ have potential applications in cell therapies aimed at limiting immune-driven pathologies.

ILC2s display significant heterogeneity and can adopt proinflammatory or tissue protective functions depending on cytokines and microenvironment factors (2, 9, 10, 12–14, 33). $ILC2_{10}$ have been shown to inhibit immune responses in diverse contexts, including inflammation in the lungs, intestines, and neurological system(9–14). In humans, individuals with grass-pollen allergies have ILC2s with reduced capacity to produce IL-10 following stimulation, and patients who respond to allergy immunotherapy have increased proportions of IL-10^+ILC2s(13). In the context of transplantation, Huang *et al.* demonstrated mouse $ILC2_{10}$ could prolong islet allograft survival by suppressing T cell attack of transplanted islets(33). These growing reports demonstrate important functions for $ILC2_{10}$ in regulating

immunity. However, to date we have lacked markers that accurately identify ILC2$_{10}$ from conventional ILC2s. In one of the few studies that attempted to identify unique markers of ILC2$_{10}$, Golebski *et al.* reported KLRG1^{+}ILC2s produced IL-10 along with other signature ILC2 cytokines(13). However, KLRG1 has also been associated with inflammatory ILC2s, and may instead mark activated or memory like ILC2 populations, not specifically ILC2$_{10}$(15–18). In our study, CITE-seq analysis of expanded human ILC2$_{10}$ revealed limited expression of KLRG1, but instead high levels of CD49d and CD86. Flow cytometry confirmed that ILC2s co-expressing CD49d and CD86 had the greatest expression of IL-10. To assess the potential broad utility of these markers, we reanalyzed the publicly available dataset from Golebski *et al* of ILCs isolated from grass-pollen allergy patients that responded to allergen immunotherapy. We show *ITGA4* (CD49d) and *CD86* increased following allergy immunotherapy, in addition to *KLRG1* previously reported. CD49d and CD86 therefore also enabled tracking expansion of ILC2$_{10}$ in a completely different context, supporting their broad utility in differentiating conventional ILC2s from ILC2$_{10}$ in human studies. *Ex vivo* expanded ILC2$_{10}$ from peripheral blood did not express KLRG1, which may indicate KLRGI is downregulated in *ex vivo* cultures, or that KLRG1 is differentially expressed by ILC2$_{10}$ in different tissues or contexts. The combination of CD49d and CD86 distinguished IL-10^{+} ILC2s from conventional ILC2s in both studies, however, and our findings support these markers can be used to isolate them or track ILC2$_{10}$ responses in human studies.

A wide range of prophylactic therapeutics have been explored to treat and prevent aGVHD, including post-transplant cyclophosphamide, calcineurin inhibitors like cyclosporine and other immunosuppressants like mycophenolate, anti-thymocyte globulin and sirolimus. While these treatments dramatically reduced incidence of aGVHD, development of aGVHD remains a major clinical challenge, affecting 30-50% of HSCT recipients(19–24). In a recent multicenter review which included a wide range of different treatment modalities, more than half of HSCT patients required a hospital stay within 100 days of transplant, with the primary reason being development of aGVHD, with severe GVHD

(grades III-IV) occurring in 41.9% of patients(20, 21). Patients diagnosed with severe aGVHD were primarily managed with increased steroid doses (51.3% of patients), however, at follow-up, 52.8% of these patients were deceased(20, 21). Therefore, novel therapies are greatly needed to improve success of HSCT.

Here we examined direct effects of $ILC2_{10}$ on allogeneic T cells that underlie GVHD pathology, which had not previously been explored. Adoptively transferred human $ILC2_{10}$ suppressed allogeneic $CD4^+$ Th1 and $CD8^+$ Tc1 cells across multiple tissue compartments, and we noted an inverse relationship between ILC2s and $CD4^+$Th1 cells in peripheral blood of HSCT recipients protected from GVHD. These findings collectively support $ILC2_{10}$ have direct suppressive capacity that can be harnessed in cell therapies, and also that $ILC2_{10}$ immunoregulatory activity extends beyond effects in the intestine. Prior mouse studies of conventional ILC2s reported ILC2-derived amphiregulin promotes intestinal repair and ILC2-mediated recruitment of MDSCs to the gut limits intestinal GVHD pathology locally, an important distinction with what we observed with human $ILC2_{10}$ (27, 46). In support of $ILC2_{10}$ having similar reparative functions to conventional ILC2s, however, expanded human $ILC2_{10}$ expressed very high levels of amphiregulin. While it would have been interesting to explore human $ILC2_{10}$ effects on MDSCs or other immune populations, this is not possible using the xenogeneic GVHD model, which is almost exclusively engrafted by human T cells, with very limited contribution from myeloid cells, NK cells or B cells. Additional protective mechanism therefore likely exist, and could be explored in humanized models that support engraftment of other immune cells in future studies. However, use of this model enabled identification direct ability of $ILC2_{10}$ to suppress allogeneic $CD4^+$ and $CD8^+$ T cells responses across multiple anatomical locations. Whether human $ILC2_{10}$-mediated T cell regulation has broader cell therapy applications in T cell-driven pathologies, such as transplant rejection or T cell-driven autoimmune disorders will be an important area to explore moving forward.

Human ILC2$_{10}$ suppress allogeneic xenoGVHD severity to similar levels as previously reported with polyclonal Tregs in this model(57). In clinical trials, evidence of Tregs limiting allo-immune responses was noted. However, use of polyclonal Tregs has not achieved significant response rates, with most patients still developing GVHD and requiring global immunosuppression(25, 26), highlighting the need for more effective therapies. We show that ILC2$_{10}$ do not inhibit T cell engraftment, as was reported with Tregs in this model (48), but instead inhibit T cell proliferation, effector functions and tissue trafficking. Therefore, ILC2$_{10}$-protective mechanisms are distinct from those observed with Treg cell therapy.

From a cell manufacturing perspective, ILC2$_{10}$ might also have several advantages over Tregs. Tregs are typically sourced from the transplant donor or recipient, necessitating time sensitive isolation and expansion(58, 59). Our study using allogeneic ILC2$_{10,}$ and a mouse study that demonstrated 3rd party ILC2s can protect from intestinal damage(27, 46) support the possibility of using 3rd party donors as an 'off-the-shelf' source of ILC2$_{10}$, which would have advantages over current Treg approaches. Further, Tregs have limited expansion potential, whereas we show ILC2$_{10}$ from peripheral blood exhibit robust expansion *ex vivo*. In addition to these cell manufacturing advantages, human ILC2$_{10}$ have very high co-expression of amphiregulin, representing another potential benefit over human Tregs, which unlike mouse Tregs do not produce amphiregulin endogenously(27, 46). It will therefore be interesting to compare and contrast ILC2$_{10}$ and Treg immunoregulatory mechanism in future studies, and explore whether dual regulatory and tissue-protective functions of human ILC2$_{10}$ could offer an additional therapeutic advantage. What is clear however, is that ILC2$_{10}$ display regulatory functions, and can limit inflammation in diverse contexts, therefore providing a strong rational to explore ILC2$_{10}$-based cell therapies for a wide range of pathologies.

Methods

490

491 **Human PBMC Isolation**

492 Fresh blood was collected in EDTA collection tubes (BD Biosciences). In some instances, frozen PBMC
493 samples were obtained from the Messner Allogeneic Transplant Program Biobank. PBMCs were
494 isolated using Lymphoprep(StemCell Technologies) per manufacturer instructions.

495

496 **Flow Cytometry**

497 Surface marker staining was performed for 30min after 15min blocking with human TruStain
498 FcX(BioLegend). Cells were washed in FACS buffer(PBS+2% FCS) and fixed in 2%paraformaldehyde
499 in PBS(ThermoFisherScientific). For intracellular staining, cells were fixed and permeabilized using
500 FOXP3/Transcription Factor Staining set(eBioscience) and incubated with intracellular antibodies at
501 room temperature(RT) for 30min. Samples were acquired on a LSR Fortessa(BD Biosciences) and data
502 analyzed using FlowJo v10 software. Antibody details listed in **Supplemental Table 3**.

503

504 **Human ILC Sorting**

505 PBMCs were stained with human TruStain FcX(BioLegend) and incubated with a cocktail of lineage
506 antibodies conjugated to the FITC listed in **Supplemental Table 4**. Cells are washed in FACS buffer,
507 resuspended in EasySep Buffer(StemCell Technologies) and enriched using the EasySep FITC Positive
508 Selection Kit II(StemCell Technologies) per manufacturer instructions. Enriched cells were stained with
509 antibody cocktail(**Supplemental Table 5**), and sorted using a FACSAria Fusion(BD Biosciences).

510

511 **Human ILC Expansion**

512 Sorted human ILC2s and ILC3s were cultured in complete X-VIVO 15 media(Lonza) supplemented with
513 5% human AB serum(Sigma), 100U/mL Penicillin-Streptomycin(Gibco) and 1x GlutaMAX(Gibco).
514 ILC2s were expanded using 100 IU/mL IL-2(SteriMax), 20ng/mL IL-7 and 20 ng/mL IL-33(BioLegend).

ILC3s were expanded using 100 IU/mL IL-2, 20ng/mL of IL-1β, IL-7 and IL-23(BioLegend). $CD56^{bright}$ and $CD56^{dim}$ NK cells were expanded in NK MACS media(Miltenyi) supplemented with 5% human AB 500 IU/mL of IL-2, and 20ng/mL of IL-15 and IL-18(Biolegend).

Cytokine and Chemokine Assays

For intracellular cytokine analysis, $2x10^5$ cells were stimulated with Cell Stimulation Cocktail(eBioscience) for 6hrs, with GolgiStop and GolgiPlug(BD Biosciences) added after 2hrs. Cells were then intracellularly stained with antibodies as detailed in **Supplemental Table 6**. For secreted factor analysis, $1x10^5$ cells were plated in complete X-Vivo media and stimulated with 100 IU/mL of IL-2. After 16hrs, supernatant was collected and stored at -80°C. Analytes were measured using the 12-plex LegendPlex Human Th Cytokine Panel(BioLegend) or the 13-plex LegendPlex Human Proinflammatory Chemokine Panel 1(BioLegend) on thawed supernatant samples per manufacturer's instructions.

Xenogeneic GVHD Mouse Model

Six-to-ten-week-old NOD.Cg-*Prkdc*^{scid}*Il2rg*^{tm1Wjl}/SzJ(NSG) mice were given 150cGy irradiation one day prior to intravenous tail vein injection of $1x10^7$ freshly isolated PBMCs with or without $1x10^7$ expanded allogeneic ILC2s in PBS at the same time or with ILC2s administered 9 days later (upon GVHD onset) (47, 60). Control mice were injected with PBS either at Day 0 or Day 9. Mice were monitored daily for symptoms of GVHD including weight loss, fur loss and skin inflammation, hunch, activity, and pain, scored on a scale of 0–3. At endpoint, blood, bone marrow and spleens were harvested as previously described(60, 61). For intestinal immune cells, intestines were flushed, sliced, and rinsed in 1xPBS. Tissue was cut into segments, added to 2mM EDTA in 1xPBS and incubated for 30min at RT. Tissue was strained and the remaining tissue was added to digestion buffer containing 1,650NPA-U BP protease(VitaCyte), 2,500CDA-U CollagenaseMA(VitaCyte), and 100µg/mL DNaseI(StemCell Technologies) in Hank's Balanced Salt Solution with calcium(Wisent Bio Products). Tissue was then cut

and incubated at 37°C for an additional 30min. Tissue was passed through a 70µm filter and washed in RPMI (Gibco)+5%FCS twice.

For graft-versus leukemia experiments, six-to-ten-week-old NSG mice were given 250cGy irradiation one day prior to intravenous tail vein injection of $2x10^6$ MV4-11 cells per mouse. Five days later, mice were given $5x10^6$ PBMCs alone or with $5x10^6$ expanded human ILC2s. Mice were sacrificed 14 days after PBMC injection, and the presence of MV4-11 cells in bone marrow was assessed.

Histology

Harvested spleen, lung and colon tissue were fixed for 3 days in 10% neutral buffered formalin and stored in 70% ethanol. Paraffin embedding, tissue slicing, H&E and immunohistochemical staining was performed by the UHN Pathology Research Program Laboratory. Quantification of cells expressing IHC markers was performed using the HALO Image Analysis Platform and reported as a percent of all cells.

Co-Cultures

Naïve $CD4^+$ and total $CD8^+$ T cells were isolated from the healthy donor blood using the EasySep Human Naïve $CD4^+$ T cell or the EasySep Human $CD8^+$ T cell isolation kit(StemCell Technologies). T cells were plated at $5x10^4$ per well and stimulated with human CD3/CD28 T-Activator DynaBeads(Gibco) at 1:8 beads:T cell ratio. Expanded ILC2s were added 1:1 to the T cells. T cells were assessed for markers after 72hrs by flow cytometry. For ILC supernatant experiments, expanded ILC2s were plated $5x10^4$ cells/mL in complete X-Vivo media without cytokines. After 16hrs, supernatant was harvested, centrifuged at 1500rpm for 10min and stored at -80°C. Supernatant was thawed on day of T cell cultures, and added 1:1 with T cells. Fresh supernatant was added every 24hrs for 3days. For inhibitor experiments, UltraLeaf anti-human IL-4, IL-9, IL-10, and IL-13(BioLegend) were added at 10µg/mL. ARL67156(Tocris) and

PBS12379(Tocris) were added at 1µg/mL to inhibit activity of CD39 and CD73, respectively. Inhibitors were added at day zero and every 24hrs for 72hrs.

CITE-seq on expanded ILCs and analysis

$1x10^6$ expanded $CD56^{bright}$, $CD56^{dim}$, ILC2s and ILC3s were washed twice in 1x Cell Staining Buffer(BioLegend) and incubated in TruStain FcX for 15min. Cells were incubated with a TotalSeq-C antibody cocktail as well as hashtag antibodies to allow for post sequencing differentiation of distinct expanded ILC subsets(BioLegend, **Supplemental Table 1**) for 30min. Antibody concentrations and background signal were determined as previously described(62). Cells were washed 3x in Cell Staining Buffer and resuspended in 1xPBS with 0.04% BSA(Millipore Sigma). Samples were prepared for sequencing using the 10X Genomics Single Cell 5' v2 platform in accordance with manufacturer's instructions for capture of 12,000 cells per samples. Reverse transcription, cDNA amplification and sequencing libraries using the 10X Genomics Single Cell 5' v2 reagents. Samples were sequenced to a depth of 40,000 reads. Read alignment to the reference human genome (GRCh38/hg38) and gene expression matrices were generated using CellRanger v6.1.2. Single cells were filtered to exclude cells that expressed >10% mitochondrial content, <1000 total transcripts and <200 unique genes. Data was log normalized, principal component analysis was preformed, and cells were clustered by the top 20 principal components with the Louvain community algorithm using Seurat's FindNeighbors and FindClusters(63). Cell cycle genes were assigned using Seurat's CellCycleScoring and regressed out during scaling. Clusters were visualized using the Uniform Manifold Approximation and Projection(UMAP)(64). Clusters were assigned to ILC subsets based on expression of hashtag antibodies, lack of lineage markers and expression of subset associated markers(**Figure 6a**). Cluster defining markers were identified using FindMarkers in Seurat. Differential expression of genes was visualized using EnhancedVolcano(65).

Data availability

CITEseq dataset of expanded human ILCs will be made publicly available via NCBI GEO at the time of publication. Publicly available single-cell RNA-sequencing dataset of ILCs in patients undergoing grass-pollen allergy immunotherapy was originally published as part of studies by Golebski *et al* (13).

Statistics

Statistical significance was determined by Kruskal-Wallis test or one-tailed Mann-Whitney test. The log-rank(Mantel-Cox) test was used for Kaplan-Meir curves. Analysis of correlational data was calculated using Spearman correlation. The number of replicates is represented by *n* and is indicated in each figure legend. *p<0.05;**P<0.01;***P<0.001;****P<0.0001;*ns,* not significant. Error bars represent standard deviation unless otherwise stated. Data analysis was preformed using GraphPad Prism v9.

Study Approval

Patient study protocols were approved by the Research Ethics Board at University Health Network in accordance with the Helsinki Declaration (UHN REB 19-6351), with all patients provided written, informed consent. Healthy peripheral blood was obtained from donors through the Canadian Blood Services Blood4Research program, with each donor providing written, informed consent(UHN REB 17-6229, CBS Approved Study 2020-047). Animal study protocols were approved by the University Health Network Animal Care Committee(UHN AUP 6203) and all ethical regulations were followed.

509 **List of Supplementary Material**

510

511 **Supplemental Figure 1. Flow cytometry gating strategy for ILC sorting**

512

513 **Supplemental Figure 2. Analysis of chemokines and cytokines produced by expanded ILC**

514 **populations**

515

516 **Supplemental Figure 3. Stability of signature cytokines on ILC2s with ILC2$_{10}$ phenotype upon**

517 **culture in different cytokine conditions**

518

519 **Supplemental Figure 4. Expression of nTreg and Tr1 markers on expanded ILCILC2s with ILC2$_{10}$**

520 **phenotype.**

521

522

523 **Supplemental Figure 5. Expanded human ILC2s suppress symptoms and improve survival of**

524 **xenogeneic GVHD in male mice**

525

526 **Supplemental Figure 6. Delayed injection of expanded human ILC2s improve weight-loss in**

527 **xenogeneic GVHD mice**

528

529 **Supplemental Figure 7. Engrafted human CD45+ cells are primarily T cells in xenogeneic GVHD**

530 **mice**

531

532 **Supplemental Figure 8. Representative flow cytometry analysis of Ki-67 and CXCR3 on CD4$^+$ and**

533 **CD8$^+$ T cells *in vivo* across tissues**

Supplemental Figure 9. Activation and checkpoint molecule expression on $CD4^+$ and $CD8^+$ T cells

Supplemental Figure 10. H&E Staining and human CD3 immunohistochemical staining tissues of xenoGVHD mouse model

Supplemental Figure 11. ILC Gating strategy to analyze ILCs in HSCT recipient peripheral blood

Supplemental Figure 12. Effect of ILC2 supernatant and addition of various inhibitors to ILC2- T cell co-cultures

Supplemental Figure 13. Non-normalized IFN-γ expression on $CD4^+$ and $CD8^+$ T cells cultured with ILC2s

Supplemental Table 1: CITE-Seq TotalSeqC antibody details

Supplemental Table 2: Patient and Healthy Donor Characteristics

Supplemental Table 3: Antibodies used for flow cytometry

Supplemental Table 4: Lineage Antibodies for ILC Sort

Supplemental Table 5: Antibodies for ILC sort

Supplemental Table 6: Intracellular Antibodies used for Flow Cytometry

559
560
561

References

1. Lim AI et al. Systemic Human ILC Precursors Provide a Substrate for Tissue ILC Differentiation. *Cell* 2017;168(6):1086-1100.e10.
2. Spits H, Mjösberg J. Heterogeneity of type 2 innate lymphoid cells. *Nat Rev Immunol* 2022;22(11):701–712.
3. Björkström NK, Kekäläinen E, Mjösberg J. Tissue-specific effector functions of innate lymphoid cells. *Immunology* 2013;139(4):416–27.
4. Vivier E et al. Innate Lymphoid Cells: 10 Years On. *Cell* 2018;174(5):1054–1066.
5. Jegatheeswaran S, Mathews JA, Crome SQ. Searching for the Elusive Regulatory Innate Lymphoid Cell. *J Immunol* 2021;207(8):1949–1957.
6. Rauber S et al. Resolution of inflammation by interleukin-9-producing type 2 innate lymphoid cells. *Nat Med* 2017;23(8):938–944.
7. Bartemes KR, Kephart GM, Fox SJ, Kita H. Enhanced innate type 2 immune response in peripheral blood from patients with asthma. *J Allergy Clin Immunol* 2014;134(3):671-678.e4.
8. Falquet M, Ercolano G, Jandus P, Jandus C, Trabanelli S. Healthy and Patient Type 2 Innate Lymphoid Cells are Differently Affected by in vitro Culture Conditions. *J Asthma Allergy* 2021;14:773–783.
9. Jegatheeswaran S, Mathews JA, Crome SQ. Searching for the Elusive Regulatory Innate Lymphoid Cell. *The Journal of Immunology* 2021;207(8):1949–1957.
10. Seehus CR et al. Alternative activation generates IL-10 producing type 2 innate lymphoid cells. *Nat Commun* 2017;8(1). doi:10.1038/s41467-017-02023-z
11. Howard E et al. IL-10 production by ILC2s requires Blimp-1 and cMaf, modulates cellular metabolism, and ameliorates airway hyperreactivity. *Journal of Allergy and Clinical Immunology* 2021;147(4):1281-1295.e5.
12. Bando JK et al. ILC2s are the predominant source of intestinal ILC-derived IL-10. *Journal of Experimental Medicine* 2020;217(2). doi:10.1084/jem.20191520
13. Golebski K et al. Induction of IL-10-producing type 2 innate lymphoid cells by allergen immunotherapy is associated with clinical response. *Immunity* 2021;54(2):291-307.e7.
14. Derecki NC et al. Meningeal Type-2 Innate Lymphoid Cells Emerge as Novel Regulators of Microglial Activation and Blood-Brain Barrier Stability: A Central Role for IL-10. *SSRN Electronic Journal* [published online ahead of print: 2019]; doi:10.2139/ssrn.3414004
15. Blanquart E et al. Targeting androgen signaling in ILC2s protects from IL-33–driven lung inflammation, independently of KLRG1. *Journal of Allergy and Clinical Immunology* 2022;149(1):237-251.e12.
16. Taylor S et al. PD-1 regulates KLRG1+ group 2 innate lymphoid cells. *Journal of Experimental Medicine* 2017;214(6):1663–1678.
17. Flamar A-L et al. Interleukin-33 Induces the Enzyme Tryptophan Hydroxylase 1 to Promote Inflammatory Group 2 Innate Lymphoid Cell-Mediated Immunity. *Immunity* 2020;52(4):606-619.e6.
18. Huang Y et al. IL-25-responsive, lineage-negative KLRG1hi cells are multipotential 'inflammatory' type 2 innate lymphoid cells. *Nat Immunol* 2015;16(2):161–169.
19. Garnett C, Apperley JF, Pavlu J. Treatment and management of graft-versus-host disease: Improving response and survival. *Ther Adv Hematol* 2013;4(6):366–378.
20. Holtan SG et al. Disease progression, treatments, hospitalization, and clinical outcomes in acute GVHD: a multicenter chart review. *Bone Marrow Transplant* 2022;57(10):1581–1585.
21. Holtan SG et al. Disease progression, hospital readmissions, and clinical outcomes for patients with steroid-refractory acute graft-versus-host disease: A multicenter, retrospective study. *Bone Marrow Transplant* 2022;57(9):1399–1404.

22. Finazzi MC et al. Characteristics of graft-versus-host disease occurring after alemtuzumab-containing allogeneic stem cell transplants: incidence, organ involvement, risk factors and survival. *Br J Haematol* 2020;188(4):550–559.
23. Jagasia M et al. Risk factors for acute GVHD and survival after hematopoietic cell transplantation. *Blood* 2012;119(1):296–307.
24. Luznik L et al. HLA-haploidentical bone marrow transplantation for hematologic malignancies using nonmyeloablative conditioning and high-dose, posttransplantation cyclophosphamide. *Biol Blood Marrow Transplant* 2008;14(6):641–50.
25. Tang Q, Bluestone JA. Regulatory T-cell therapy in transplantation: moving to the clinic.. *Cold Spring Harb Perspect Med* 2013;3(11). doi:10.1101/cshperspect.a015552
26. Duggleby R, Danby RD, Madrigal JA, Saudemont A. Clinical Grade Regulatory CD4+ T Cells (Tregs): Moving Toward Cellular-Based Immunomodulatory Therapies. *Front Immunol* 2018;9:252.
27. Bruce DW et al. Type 2 innate lymphoid cells treat and prevent acute gastrointestinal graft-versus-host disease. *Journal of Clinical Investigation* 2017;127(5):1813–1825.
28. Piperoglou C et al. Innate lymphoid cell recovery and occurrence of GvHD after hematopoietic stem cell transplantation [Internet]. *J Leukoc Biol* 2022;111(1):161–172.
29. Kroeze A et al. Presence of innate lymphoid cells in allogeneic hematopoietic grafts correlates with reduced graft-versus-host disease. *Cytotherapy* 2022;24(3):302–310.
30. Simonetta F, Alvarez M, Negrin RS. Natural killer cells in graft-versus-host-disease after allogeneic hematopoietic cell transplantation. *Front Immunol* 2017;8(APR). doi:10.3389/fimmu.2017.00465
31. Minculescu L et al. Early Natural Killer Cell Reconstitution Predicts Overall Survival in T Cell–Replete Allogeneic Hematopoietic Stem Cell Transplantation. *Biology of Blood and Marrow Transplantation* 2016;22(12):2187–2193.
32. Marius Munneke J et al. Activated innate lymphoid cells are associated with a reduced susceptibility to graft-versus-host disease. *Blood* 2014;124(5):812–821.
33. Huang Q et al. IL -10 producing type 2 innate lymphoid cells prolong islet allograft survival. *EMBO Mol Med* 2020;12(11). doi:10.15252/emmm.202012305
34. Chen PP et al. Alloantigen-specific type 1 regulatory T cells suppress through CTLA-4 and PD-1 pathways and persist long-term in patients. *Sci Transl Med* 2021;13(617). doi:10.1126/scitranslmed.abf5264
35. Gagliani N et al. Coexpression of CD49b and LAG-3 identifies human and mouse T regulatory type 1 cells. *Nat Med* 2013;19(6):739–746.
36. Long A et al. Type 2 Innate Lymphoid Cells Impede IL-33-Mediated Tumor Suppression. *J Immunol* 2018;201(11):3456–3464.
37. Ohta A et al. A2A Adenosine Receptor May Allow Expansion of T Cells Lacking Effector Functions in Extracellular Adenosine-Rich Microenvironments. *The Journal of Immunology* 2009;183(9):5487–5493.
38. Long A et al. Type 2 Innate Lymphoid Cells Impede IL-33–Mediated Tumor Suppression. *The Journal of Immunology* 2018;201(11):3456–3464.
39. Murphy JM, Ngai L, Mortha A, Crome SQ. Tissue-Dependent Adaptations and Functions of Innate Lymphoid Cells. *Front Immunol* 2022;13:836999.
40. Mak ML, Reid KT, Crome SQ. Protective and pathogenic functions of innate lymphoid cells in transplantation. *Clin Exp Immunol* [published online ahead of print: April 29, 2023]; doi:10.1093/cei/uxad050
41. Burman AC et al. IFNγ differentially controls the development of idiopathic pneumonia syndrome and GVHD of the gastrointestinal tract. *Blood* 2007;110(3):1064–1072.
42. Guy-Grand D, Vassalli P. Gut injury in mouse graft-versus-host reaction. Study of its occurrence and mechanisms. *Journal of Clinical Investigation* 1986;77(5):1584–1595.

43. Gutiérrez-Hoya A et al. Role of CD8 Regulatory T Cells versus Tc1 and Tc17 Cells in the Development of Human Graft-versus-Host Disease. *J Immunol Res* 2017;2017. doi:10.1155/2017/1236219
44. Szebeni J, Wang MG, Pearson DA, Szot GL, Sykes M. IL-2 inhibits early increases in serum gamma interferon levels associated with graft-versus-host-disease. *Transplantation* 1994;58(12):1385–93.
45. Xhaard A et al. Steroid-Refractory Acute GVHD: Lack of Long-Term Improved Survival Using New Generation Anticytokine Treatment. *Biology of Blood and Marrow Transplantation* 2012;18(3):406–413.
46. Bruce DW et al. Third-party type 2 innate lymphoid cells prevent and treat GI tract GvHD. *Blood Adv* 2021;5(22):4578–4589.
47. Ehx G et al. Xenogeneic Graft-Versus-Host Disease in Humanized NSG and NSG-HLA-A2/HHD Mice. *Front Immunol* 2018;9. doi:10.3389/fimmu.2018.01943
48. Proics E et al. Preclinical assessment of antigen-specific chimeric antigen receptor regulatory T cells for use in solid organ transplantation. *Gene Ther* 2023;30(3–4):309–322.
49. Choi J et al. *IFNR signaling mediates alloreactive T-cell trafficking and GVHD [Internet]*. 2012:
50. Croudace JE et al. Chemokine-mediated tissue recruitment of CXCR3+ CD4+ T cells plays a major role in the pathogenesis of chronic GVHD. *Blood* 2012;120(20):4246–55.
51. Crome SQ, Wang AY, Kang CY, Levings MK. The role of retinoic acid-related orphan receptor variant 2 and IL-17 in the development and function of human CD4+ T cells. *Eur J Immunol* 2009;39(6):1480–1493.
52. Crome SQ et al. Inflammatory Effects of Ex Vivo Human Th17 Cells Are Suppressed by Regulatory T Cells. *The Journal of Immunology* 2010;185(6):3199–3208.
53. Acosta-Rodriguez E v. et al. Surface phenotype and antigenic specificity of human interleukin 17-producing T helper memory cells. *Nat Immunol* 2007;8(6):639–646.
54. Cosmi L et al. CRTH2 is the most reliable marker for the detection of circulating human type 2 Th and type 2 T cytotoxic cells in health and disease. *Eur J Immunol* 2000;30(10):2972–9.
55. Murphy KM, Reiner SL. The lineage decisions of helper T cells. *Nat Rev Immunol* 2002;2(12):933–944.
56. Yang L et al. Interleukin-13 interferes with activation-induced t-cell apoptosis by repressing p53 expression. *Cell Mol Immunol* 2016;13(5):669–77.
57. Reading JL et al. Augmented Expansion of Treg Cells From Healthy and Autoimmune Subjects via Adult Progenitor Cell Co-Culture. *Front Immunol* 2021;12:716606.
58. Hefazi M, Bolivar-Wagers S, Blazar BR. Regulatory T Cell Therapy of Graft-versus-Host Disease: Advances and Challenges. *Int J Mol Sci* 2021;22(18). doi:10.3390/ijms22189676
59. McCallion O, Bilici M, Hester J, Issa F. Regulatory T-cell therapy approaches. *Clin Exp Immunol* 2023;211(2):96–107.
60. Dawson NAJ et al. Systematic testing and specificity mapping of alloantigen-specific chimeric antigen receptors in regulatory T cells. *JCI Insight* 2019;4(6). doi:10.1172/jci.insight.123672
61. Liu X, Quan N. Immune Cell Isolation from Mouse Femur Bone Marrow. *Bio Protoc* 2015;
62. Colpitts SJ et al. Strategies for optimizing CITE-seq for human islets and other tissues.. *Front Immunol* 2023;14:1107582.
63. Hao Y et al. Integrated analysis of multimodal single-cell data. *Cell* 2021;184(13):3573-3587.e29.
64. McInnes L, Healy J, Saul N, Großberger L. UMAP: Uniform Manifold Approximation and Projection. *J Open Source Softw* 2018;3(29):861.
65. Blighe K, Rana S, Lewis M. EnhancedVolcano: publication-ready volcano plots with enhanced colouring and labeling. Bioconductor version: Release (3.11), 2020

Acknowledgments

First and foremost, we would like to thank the HSCT patients at UHN who made this work possible. We would also like to thank the nurses and physicians and surgeons at Princess Margaret Cancer Centre for efforts to obtain samples, and acknowledge technical support provided by the Princess Margaret Genomics Centre, particularly Troy Ketela and Julissa Tsao, the Princess Margaret Cancer Centre flow cytometry core and the UHN Pathology Research Program laboratory. We thank Drs Slava Epelman and Clint Robbins for helpful feedback on the manuscript. Schematic figures were created with BioRender.com. KTR is supported by a MITACs Accelerate award. SJC was supported by a Banting and Best Novo Nordisk Scholarship and a Queen Elizabeth II/Dr. Dina Gordon Malkin Graduate Scholarship in Science and Technology. JMM is supported by Ontario Graduate Scholarships, QE II/Aventis Pasteur Graduate Scholarship and a Peterborough. K.M. Hunter Foundation Scholarship. JM is supported by the Gloria and Seymour Epstein Chair in Cell Therapy and Transplantation. SQC is a Tier 2 Canada Research Chair in Tissue-Specific Immune Tolerance. This research was supported by funding from the Canadian Institutes for Health Research (169084) and Natural Sciences and Engineering Research Council of Canada. SQC was also supported by the Medicine by Design program (Canada First Research Excellence Fund), the Ajmera Transplant Centre and Canada Foundation for Innovation grant 38308. We are grateful to Canadian Blood Services and donors for providing research samples for completion of this project. The reporting and interpretation of research findings are the responsibility of the authors, the views expressed herein do not necessarily represent the view of Canadian Blood Services.

Author contributions

KTR, ASC, JM and SQC designed patient-based studies. KTR, JBL, LZ and SQC designed and implemented xenogeneic GVHD studies. JM established the Hans Messner biobank and the infrastructure required. ASC, INB, TAM and JM liaised with patient care teams to obtain human samples

for study. KTR, JAM, JMM, SJC and SQC developed ILC isolation and expansion methods. KTR, SJC, JAM, JMM, DTB, WC, NS, JA, and YX performed experiments and analysed data. KTR, SJC, JMM and SQC designed and implemented the bioinformatic pipeline for scCITEseq. SQC, JBL, AM, LZ and JM supervised the work. KTR and SQC wrote the manuscript, which all authors reviewed and edited.

Competing interests

Authors declare that they have no competing financial interests. KTR, SJC, JAM, JMM and SQC have filed a provisional patent for human ILC expansion methods (Provisional Patent Application#: 63/353,823) and KTR, SJC, WC and SQC have filed a provisional patent for marker combinations for $ILC2_{10}$ isolation (Provisional Patent Application#: 63/469,234)

Materials and correspondence

Correspondence and requests for materials should be addressed to Sarah Crome (sarah.crome@utoronto.ca).

Figures

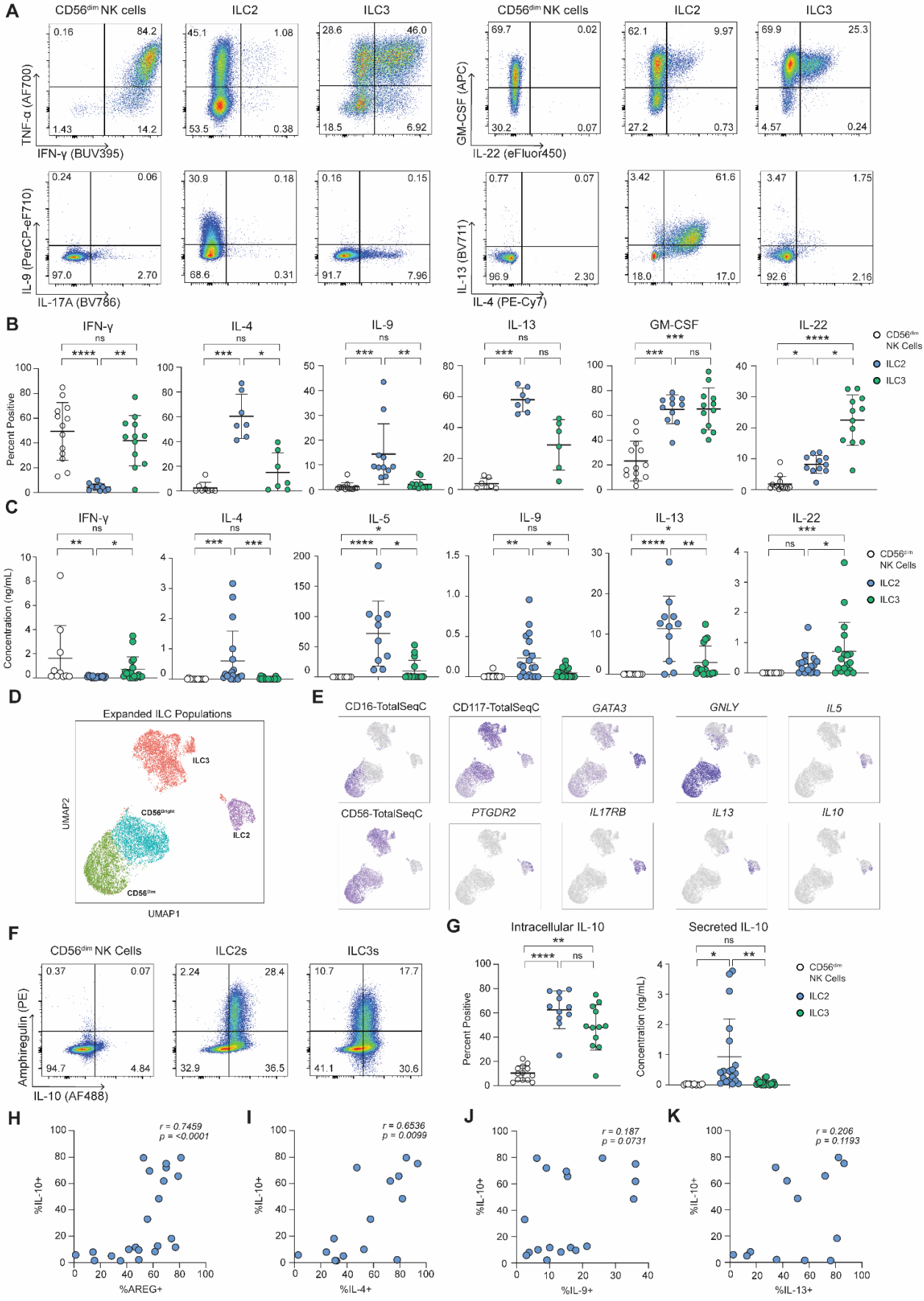

Figure 1. Expanded human ILC2$_{10}$ maintain expression of signature cytokines. To explore the role of human ILC2s in GVHD, human ILCs were isolated from peripheral blood using flow cytometry and expanded *ex vivo* using ILC subset-specific cytokines, as ILC2s are present in very low abundance in peripheral blood. ILC2s expanded using our approach displayed and ILC2$_{10}$ phenotype. Representative (**A**) and average (**B**) of intracellular cytokine staining for signature cytokines in CD56^{dim} NK cells, ILC2s and ILC3s at day 20 of expansion after stimulation with phorbol 12-myristate 13-acetate(PMA) and ionomycin. (**C**) Cytometric bead array analysis of secreted cytokines after plating ILCs at a concentration of 2x10^5 cells/mL for 16-hour stimulation with 100U/mL of IL-2. (**D**) UMAP representation of CITE-seq of expanded ILC subsets. ILC subsets indicated were isolated by flow cytometry, expanded and then stained with CITE-seq antibody cocktail as outlined in **Supplemental Table 2**. Each population was also labeled with a unique hashtag antibody to facilitate post sequencing identification. (**E**) Feature plots showing protein level expression of CD16, CD56 and CD117 and RNA level expression of *PTGDR2, GATA3, IL17RB, GNLY, IL13, IL5* and *IL-10* on expanded ILC subsets. (**F**) Representative intracellular IL-10 and amphiregulin expression by expanded CD56^{dim} NK cells, ILC2s and ILC3s after PMA/Ionomycin stimulation. (**G**) Average intracellular IL-10 expression assessed by flow cytometry (n=13, 11 and 12 for CD56^{dim} NK cells, ILC2s and ILC3s respectively) and secreted IL-10 by cytometric bead array by expanded ILC subsets (n=12, 19 and 20 for CD56^{dim} NK cells, ILC2s and ILC3s respectively). Correlation of IL-10 expression with amphiregulin (**G**), IL-4 (**H**), IL-9 (**J**) or IL-13 (**K**)(n=22, 15, 18 and 13 respectively) on expanded ILC2s with ILC2$_{10}$ phenotype.

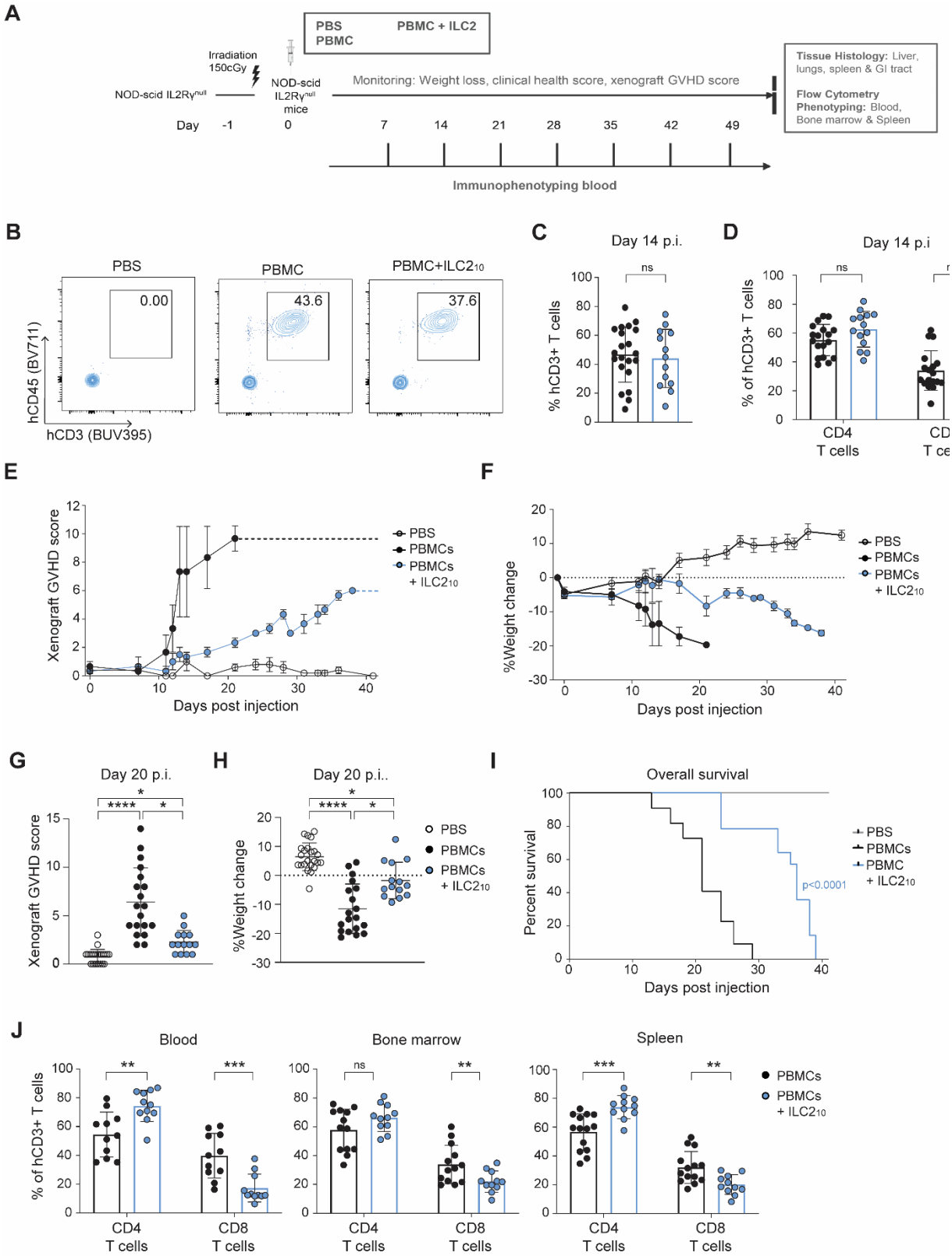

Figure 2. Cell therapy with human ILC2$_{10}$ suppresses xenogeneic GVHD. To assess whether human ILC2$_{10}$ could limit GVHD, we employed an established xenogeneic model of GVHD involving PBMC transfer into NOD-scid-IL2Rg^{null} mice (NSG). (**A**) Overview of the xenogeneic GVHD model to assess whether ILC2$_{10}$ would prophylactically limit GVHD. Briefly, NSG mice are irradiated and receive either PBS, human PBMCs, to induce multiorgan tissue pathology, or PBMCs and ILC2$_{10}$ together. Mice are

monitored for symptoms of xenogeneic GVHD including weight loss, survival and a composite xenogeneic GVHD score consisting of hunch, skin inflammation and fur loss, activity, pain and percent weight change. Blood is drawn at 7-day intervals for confirmation of human immune cell engraftment and immunophenotyping. At the humane or experimental endpoint, mice are euthanized, and tissues collected for histology or flow cytometry analysis. (**B**)Representative engraftment human $CD3^+$ $CD45^+$ T cells at day 14 post injection of human PBMCs alone or with $ILC2_{10}$. **C**,**D** Average engraftment of human $CD3^+$ $CD45^+$ (**C**), or $CD4^+$ and $CD8^+$ T cells (**D**), in the blood 14 days post injection across 3 independent experiments (n=21 for NSG mice receiving human PBMC and n=13 for NSG mice receiving human PBMC plus allogeneic $ILC2_{10}$ mice from 3 independent experiments). **E,F** (**E**) Representative xenogeneic GVHD score (n=3/group in this experiment), and (**F**) representative weight loss (n=3/group in this experiment) of 3 independent experiments. **G,H** Average of xenogeneic (**G**) GVHD score and (**H**) weight loss of mice at day 20 post injection across three independent experiments (n=23 for PBS treated NSG mice, n=19 for NSG mice receiving human PBMCs alone and n=14 for NSG mice receiving human PBMC plus allogeneic $ILC2_{10}$ respectively across 3 independent experiments). (**I**) Survival of mice treated with $ILC2_{10}$ across 3 independent experiments (n=23, 19 and 14 for NSG mice receiving PBS, PBMC and PBMC+ $ILC2_{10}$ respectively). Experimental endpoint was day 40 for any mice not reaching human endpoint. (**J**) Average proportion of $CD4^+$ and $CD8^+$ T cells of total human $CD3^+$ T cells in the blood, bone marrow and spleens of NSG mice at endpoint (n=11 and 13 from PBMC and PBMC+ $ILC2_{10}$ respectively from 3 independent experiments).

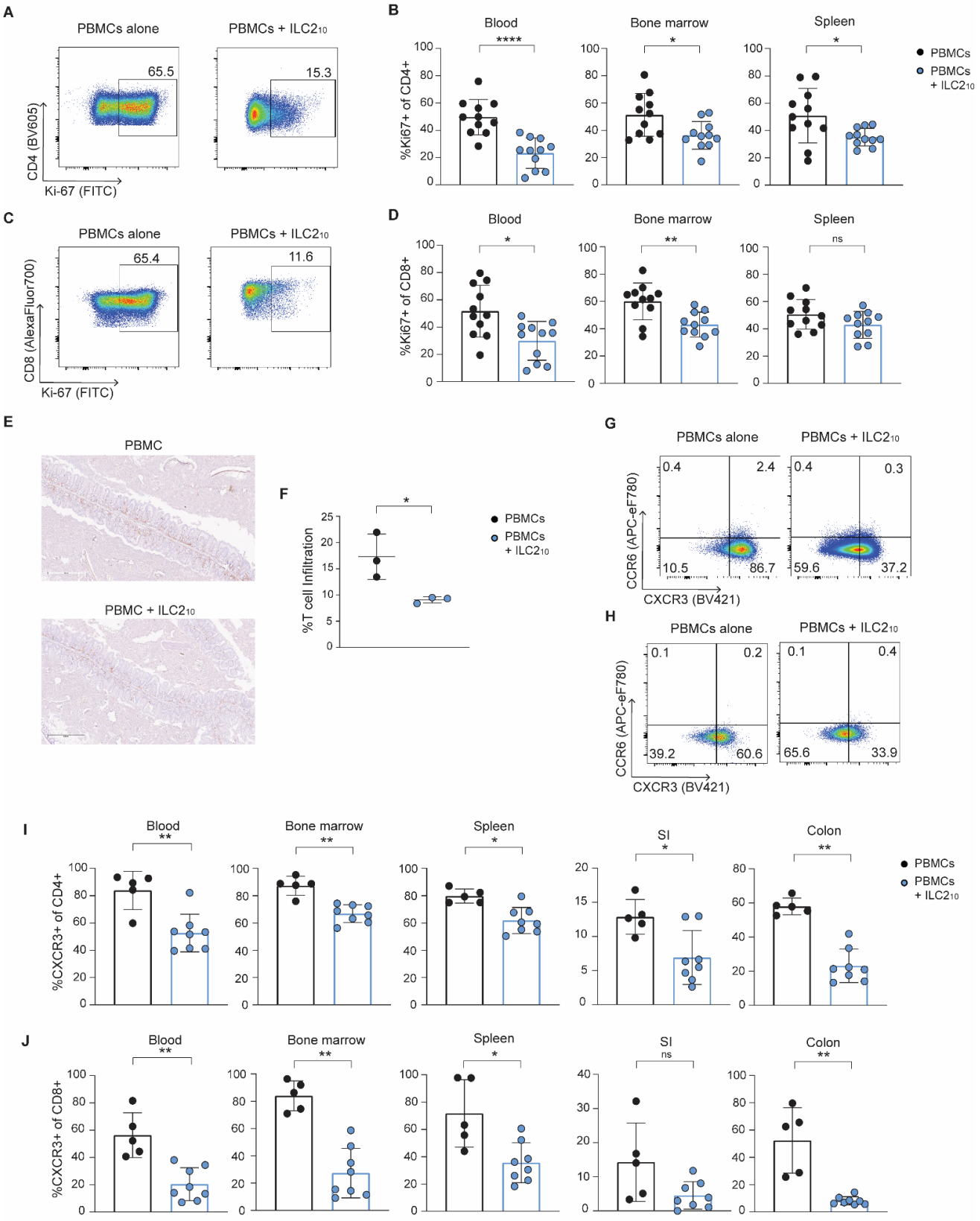

Figure 3. Cell therapy with ILC2$_{10}$ suppresses CD4$^+$ and CD8$^+$ T cell proliferation, intestinal infiltration and CXCR3 expression. Effect of ILC2$_{10}$ transfer on T cell phenotypes and proliferation in xenogeneic GVHD model were assessed by flow cytometry at endpoint. (**A**) Representative Ki-67

expression by circulating human $CD4^+$ T cells from the blood at end point (**B**) Average Ki-67 expression in blood, bone marrow or spleen at endpoint by human $CD4^+$ T cells from 3 independent experiments(n=11 mice per condition from 3 independent experiments). (**C**) Representative Ki-67 expression by circulating human $CD8^+$ T cells. (**D**) Average Ki-67 expression in the blood, bone marrow or spleen at endpoint on human $CD8^+$ T cells from 3 independent experiments(n=11 mice per condition from 3 independent experiments) (**E**) Representative human CD3 immunohistochemistry of the colon of mice treated with PBMCs or PBMCs plus $ILC2_{10}$ (10x magnification). (**F**) Average T cell infiltration in the colon of mice treated with PBS, PBMCs or PBMCs + $ILC2_{10}$. Quantified using CD3 immunohistochemistry and the HALO algorithm and normalized to background in PBS mice. **G,H** Representative CXCR3 expression on circulating human $CD4^+$ (**G**) or $CD8^+$ (**H**) T cells. Average CXCR3 expression on human $CD4^+$ (**I**) or $CD8^+$ (**j**) T cells in the blood, bone marrow, spleen, colon, and small intestines at experimental endpoint (n=5 from 2 independent experiments).

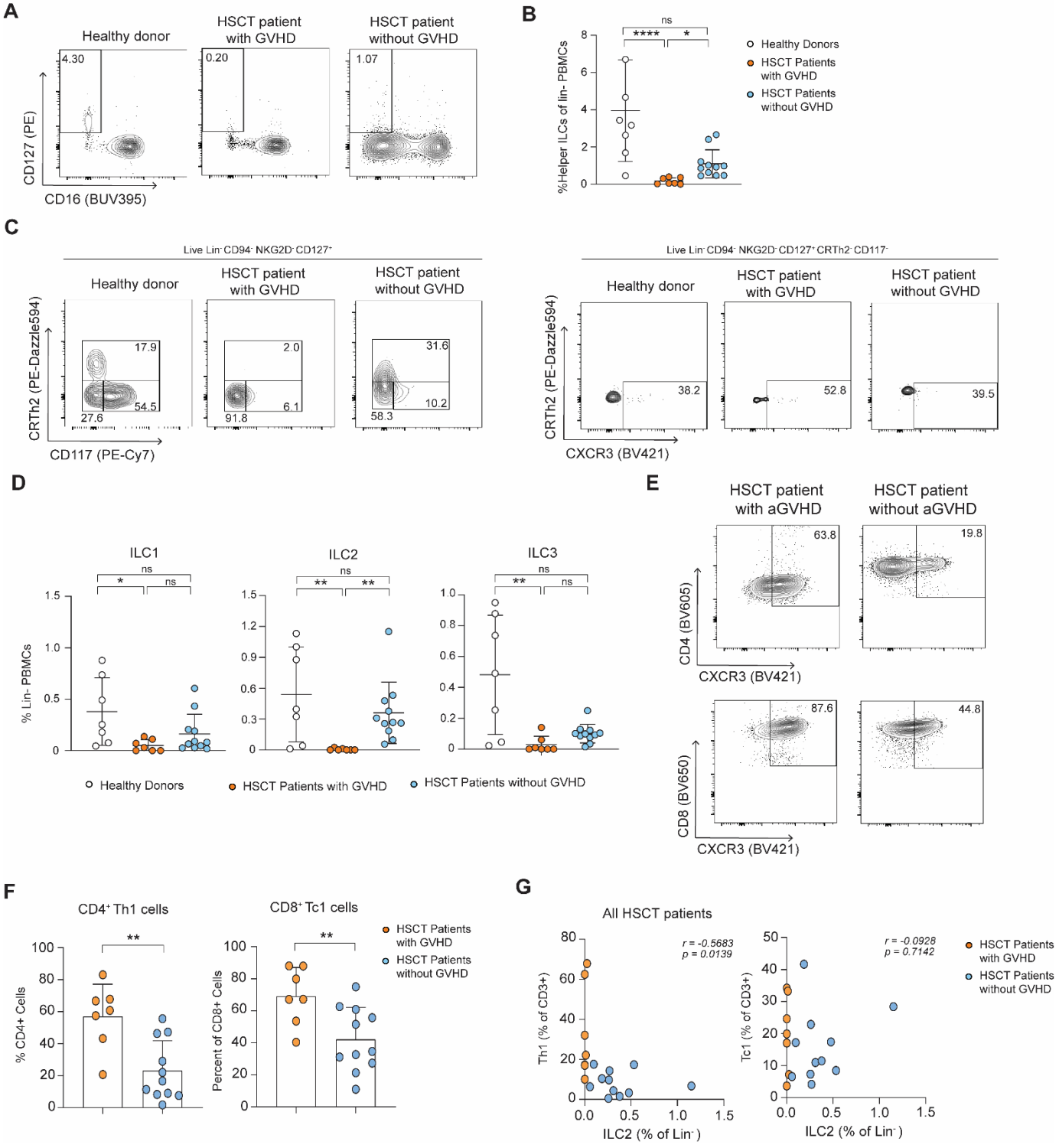

Figure 4. Increased circulating ILC2s is associated with decreased CD4$^+$ Th1 cells in HSCT recipients protected from GVHD. PBMCs from healthy donors, and HSCT patients with or without GVHD were assessed for ILC proportions and phenotypes using flow cytometry. **A,B** Representative flow plots (**A**) and summary graphs (**B**) of total CD127$^+$ helper ILCs in PBMCs as a proportion of live CD45$^+$ lineage negative cells. Lineage markers are CD3, CD4, CD8, CD14, CD19, CD20, CD33, CD34, CD123, CD138, CD303, FCεRI and TCR$\gamma\delta$. **C,D** Representative (**C**) and average (**D**) CD117$^-$, CRTh2$^-$, CXCR3$^+$ ILC1s, CRTh2$^+$ ILC2s and CRTh2$^-$ CD117$^+$ ILC3s in PBMCs as a proportion of live CD45$^+$ lineage negative cells. (**E**) Representative CD4$^+$ Th1 and CD8$^+$ Tc1 cells in HSCT patients with or without aGVHD

development. (**F**) CD4$^+$ Th1 and CD8$^+$ Tc1 cells across HSCT patients as a proportion of CD4$^+$ and CD8$^+$ T cells respectively. (**G**) Correlation of Th1 and Tc1 cells with ILC2s across all HSCT patients.

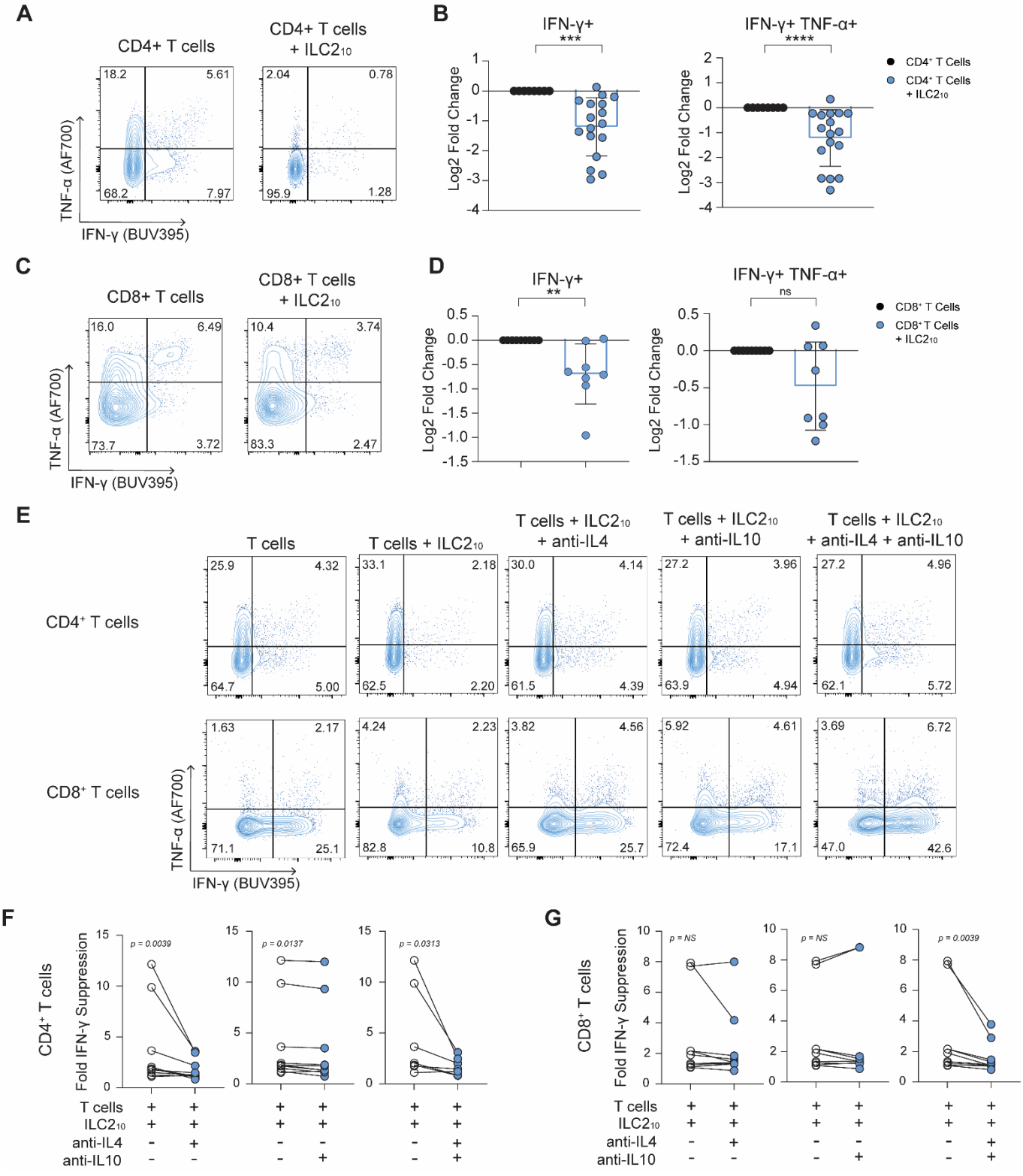

Figure 5. ILC2$_{10}$ suppress CD4$^+$ and CD8$^+$ T cell cytokine production via a combination of IL-4 and IL-10. To determine whether cell therapy with ILC2$_{10}$ protective effects were due to direct effects of ILC2$_{10}$on allogeneic CD4$^+$ and CD8$^+$ T cells, we performed *in vitro* co-cultures. Expanded ILC2$_{10}$ were

940 cultured with naïve $CD4^+$ and $CD8^+$ T cells that were activated with anti-CD3/anti-CD28 beads. After 4
941 days in culture, intracellular cytokine staining was assessed by flow cytometry. (**A**) Representative IFN-γ
942 and TNF-α expression by naïve $CD4^+$ T cells cultured with or without allogeneic $ILC2_{10}$ at day 4. (**B**)
943 Average decrease in IFN-γ production or IFN-γ and TNF-α co-expression represented as log_2fold change
944 compared to $CD4^+$ T cells alone (n=17). (**C**) Representative IFN-γ and TNF-α expression on $CD8^+$ T cells
945 co-cultured with allogeneic $ILC2_{10}$ and stimulated with anti-CD3/CD28 beads over 4 days by
946 representative flow cytometry plots. (**D**) Average decrease in IFN-γ and co-expression of IFN-γ and TNF-
947 α representative as log_2fold change compared to $CD8^+$ T cells alone (n=8). (**E**) Representative $CD4^+$ and
948 $CD8^+$ T cell IFN-γ expression when cultured with or without $ILC2_{10}$ in the presence of indicated blocking
949 anti-IL-4 and/or anti-IL-10 antibodies. Effects on fold change in IFN-γ expression by $CD4^+$ (**F**) or $CD8^+$
950 (**G**) T cells after culture with $ILC2_{10}$ with the addition of anti-IL-4 (n=10), anti-IL-10 (n = 10) or anti-IL-
951 4 and anti-IL-10 (n=7) blocking antibodies
952

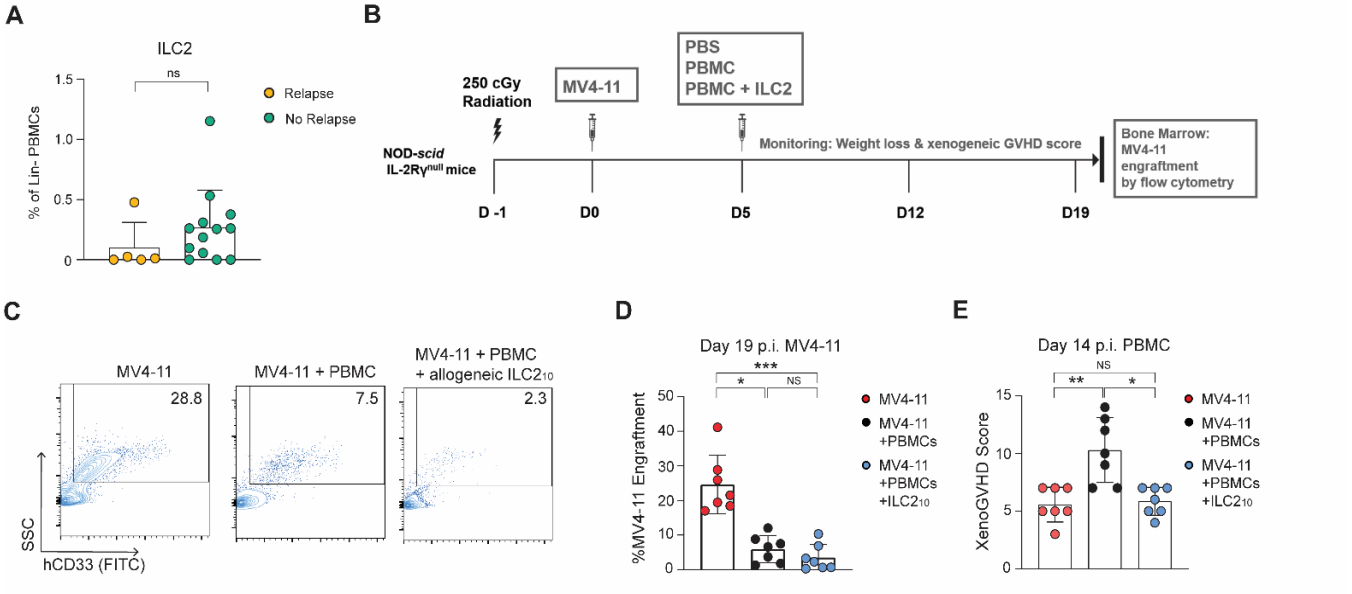

Figure 6. Cell therapy with ILC2$_{10}$ does not impede T cell-mediated graft-versus-leukemia effect. (A) Circulating ILC2s from HSCT patients as a proportion of lineage negative PBMCs. Patients were grouped based on whether they experienced cancer relapse (n=5) or not (n=13). Follow up periods at time of assessment ranged from 30 to 120 days. (**B**) Overview of humanized GVL model, whereby MV4-11 AML cells are transplanted into NSG mice. PBMCs are administered at D5 following MV4-11 transfer, and engrafted T cells reduced MV4-11 cell engraftment. (**C**) Representative MV4-11 cells in bone marrow of NSG mice treated with PBS, PBMCs or PBMCs with ILC2$_{10}$. (**D**) Average MV4-11 engraftment in NSG mice treated with PBS, PBMCs or PBMCs with ILC2$_{10}$ from two independent experiments (n=7/group) (**E**) Average xenogeneic GVHD score at day 19 from 2 independent experiments (n = 7/group). Day 19 corresponded to 14 days following injection of PBMCs with or without ILC2$_{10}$.

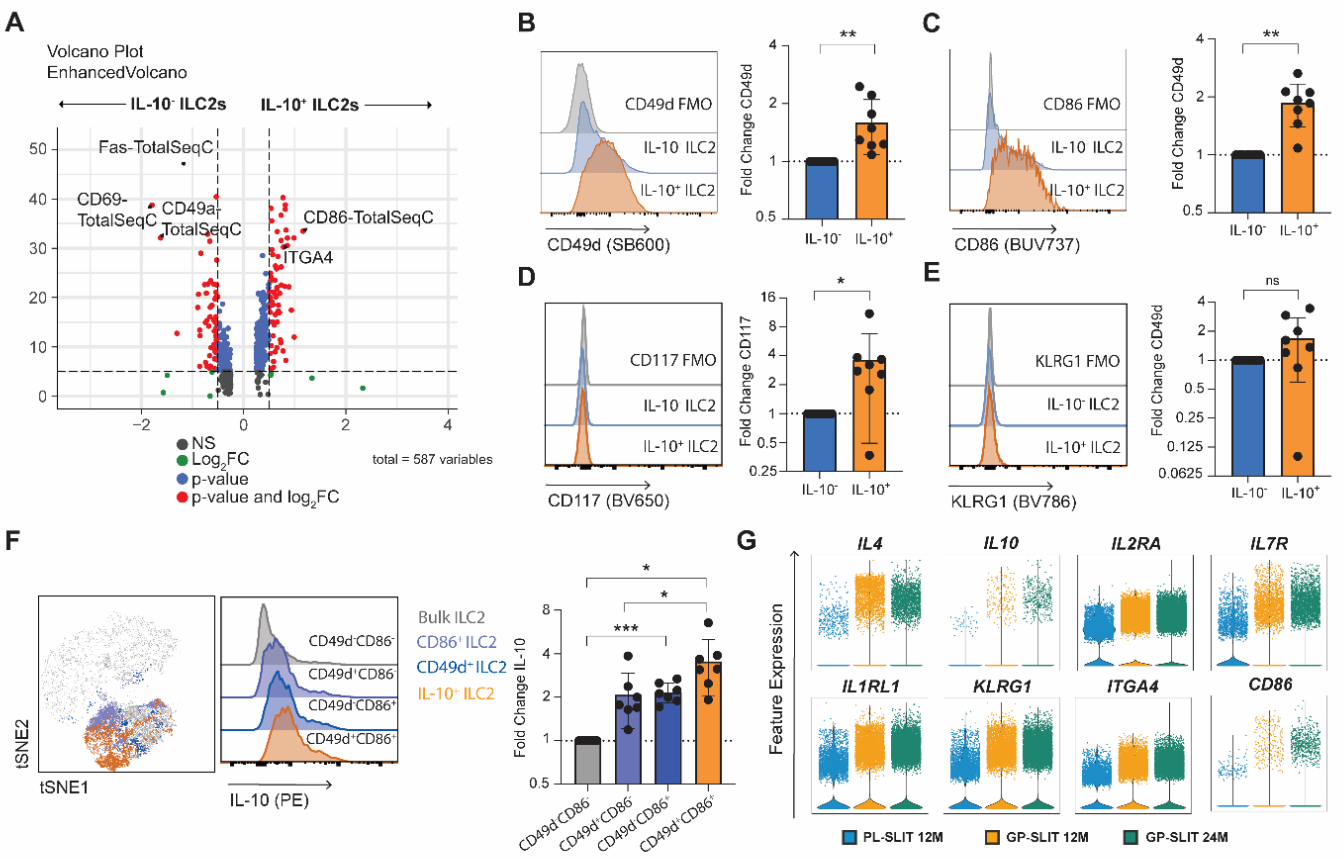

Figure 7. CD49d and CD86 mark human ILC2$_{10}$. (**A**) Volcano plot of top differentially expressed transcripts and antibody-derived tags (ADT) between IL-10$^+$ and IL-10$^-$ expanded human ILC2s. To validate uniquely expressed surface markers of ILC2$_{10}$, flow cytometry was performed on additional donors for CD49d CD86. **B-E**, Representative and average expression of CD49d (**B**), CD86 (**C**), as well as CD117 (**D**), and KLRG1 (**E**) by IL-10$^+$ and IL-10$^-$ ILC2s following PMA/ionomycin stimulation (n=7). (**F**) Average expression of IL-10 following PMA-ionomycin stimulation on ILC2s based on expression of CD49d and CD86 as a representative IL-10 expression, tSNE clustering based on co-expression and average graphs (n=7). (**G**) Violin plots of gene expression of CD86 and CD49d, as well as other ILC2$_{10}$-associated molecules, from publicly available scRNAseq dataset of grass-pollen allergy patients treated with placebo (PL-SLIT) or grass-pollen allergen immunotherapy (GP-SLIT) at 12 or 24 month follow-up (n = 2 patients per group).

Supplementary Materials

Cell therapy with IL-10-producing group 2 innate lymphoid cells suppresses Graft-versus-Host disease

Kyle T. Reid[1,2], Sarah J. Colpitts[1,2], Jessica A. Mathews[2], Abel Santos Carreira[3], Julia M. Murphy[1,2], Dorota T. Borovsky[1], Wenhui Cui[1,2], Tommy Alfaro Moya[3,4], Nadia Sachewsky[2], James An[1,2], Yubing Xia[1,2], Arthur Mortha[1], Jong Bok Lee[2], Li Zhang[1,2,5], Igor Novitzky-Basso[1,3], Jonas Mattsson[1,3], and Sarah Q. Crome[1,2]

[1]Department of Immunology, Temerty Faculty of Medicine, University of Toronto, Toronto, Canada

[2]Toronto General Hospital Research Institute, Ajmera Transplant Centre, University Health Network, Toronto, Canada

[3]Princess Margaret Cancer Centre, University Health Network, Toronto, Canada

[4]Postgraduate Medical Education Program, Temerty Faculty of Medicine, University of Toronto, Toronto, Canada

[5]Department of Laboratory Medicine and Pathology, Temerty Faculty of Medicine, University of Toronto, Toronto, Canada

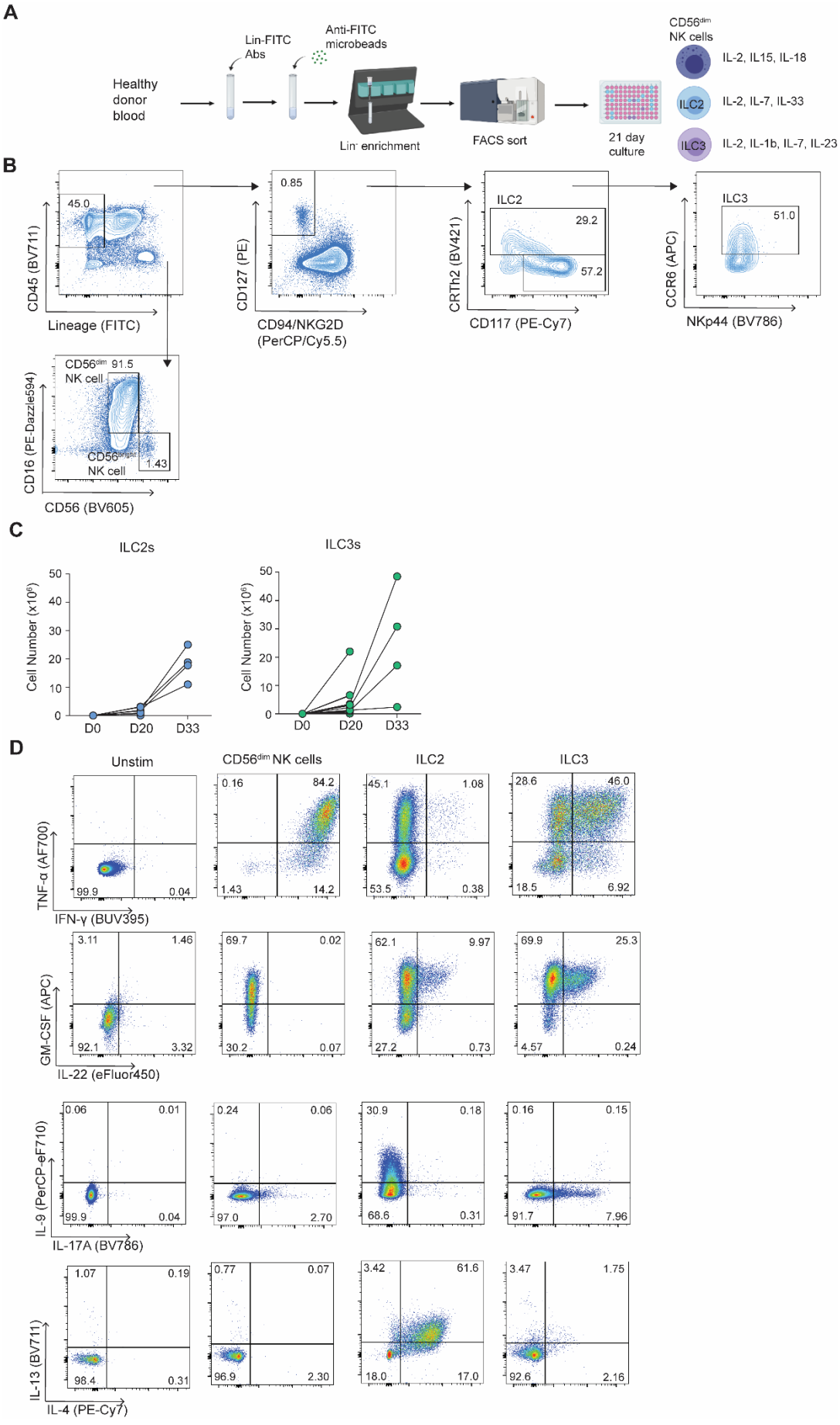

Supplemental Figure 1. Flow cytometry gating strategy for ILC sorting. To explore the role of human ILC2s in GVHD, human ILCs had to be isolated from peripheral blood using flow cytometry and expanded ex vivo using ILC subset-specific cytokines as they are present in very low abundance in peripheral blood. (A) Overview of isolation and expansion of human ILC subsets. Briefly, total PBMCs are isolated from healthy donor blood. PBMCs are incubated with FITC-conjugated linage antibodies. Lineage antibodies added are CD3 (OKT3), CD3 (UCHT1), CD4, CD8a, CD14, CD15, CD19, CD20, TCRαβ, TCR$\gamma\delta$, CD33, CD34, CD203c, FCεRI, CD79a and CD138. Anti-FITC magnetic microbeads are added, and cells are enriched for lineage$^-$ cells using StemCell magnets. Enriched cells are FACS sorted for CD56^{dim} NK cells, ILC2s and ILC3s. ILC2s are cultured with 100U/mL IL-2, 10ng/mL IL-7 and 10ng/mL IL-33, ILC3s are cultured with 100U/mL IL-2, 10ng/mL IL-7, 10ng/mL IL-1β, and 10ng/mL of IL-23 and CD56^{dim} NK cells are cultured with 500U/mL IL-2, 10ng/mL IL-15, and 10ng/mL of IL-18. (**B**) Representative gating strategy for ILC subsets. All ILCs are gated as Live, CD45$^+$ and Lin$^-$. NK cells are then gating as CD56$^+$ CD16$^+$ for CD56^{dim} NK cells and CD56^{bright} CD16$^-$ for CD56^{bright} NK cells. Helper ILCs are then sorted as live, lineage$^-$ CD94$^-$NKG2D$^-$CD127$^+$ with ILC2s being CRTh2$^+$ CCR6$^-$ and ILC3s being CRTh2$^-$CD117$^+$CCR6$^+$. (**C**) Cell expansion yields of ILC2s and ILC3s at day 20 and day 33. (**D**) Expanded ILCs intracellular cytokine staining with unstimulated ILCs as the gating control.

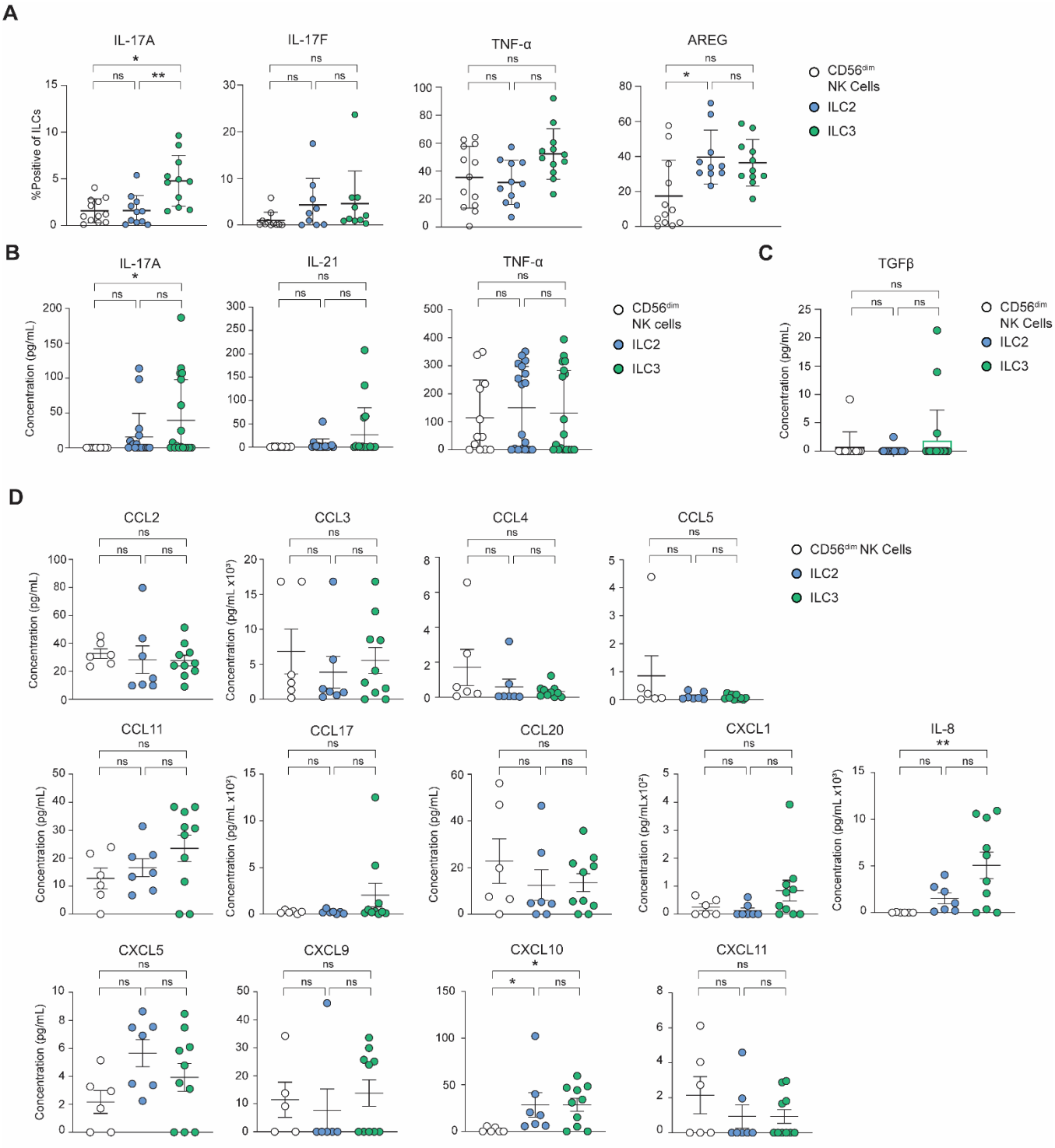

Supplemental Figure 2. Analysis of chemokines and cytokines produced by expanded ILC populations. Further chemokine and cytokine analysis of ILC2s with an $ILC2_{10}$ phenotype, as compared to NK cells and ILC3s**.** (**A**) Intracellular cytokine staining for IL-17A, IL-17F, TNF-α and Amphiregulin after 6-hour stimulation with phorbol 12-myristate 13-acetate and ionomycin and blocked with monensin and brefeldin A (n=13, 11 and 12 for $CD56^{dim}$ NK cells, ILC2s and ILC3s respectively). (**B**) Cytometric bead array (CBA) analysis of secreted IL-17A, IL-21, and TNF-α after plating ILCs at a concentration of $2x10^5$ cells/mL for 16-hour stimulation with 100U/mL of IL-2 (n=13, 18 and 18 for $CD56^{dim}$ NK cells,

ILC2s and ILC3s respectively). (**C**) CBA analysis of secreted active TGF-β1 after plating ILCs at a concentration of $2x10^5$ cells/mL for 16-hour stimulation with 100U/mL of IL-2 (n=13, 18 and 18 for $CD56^{dim}$ NK cells, ILC2s and ILC3s respectively). (**D**) CBA analysis of secreted chemokines after plating ILCs at a concentration of $2x10^5$ cells/mL for 16-hour stimulation with 100U/mL of IL-2. (n=6, 7 and 10 for $CD56^{dim}$ NK cells, ILC2s and ILC3s respectively).

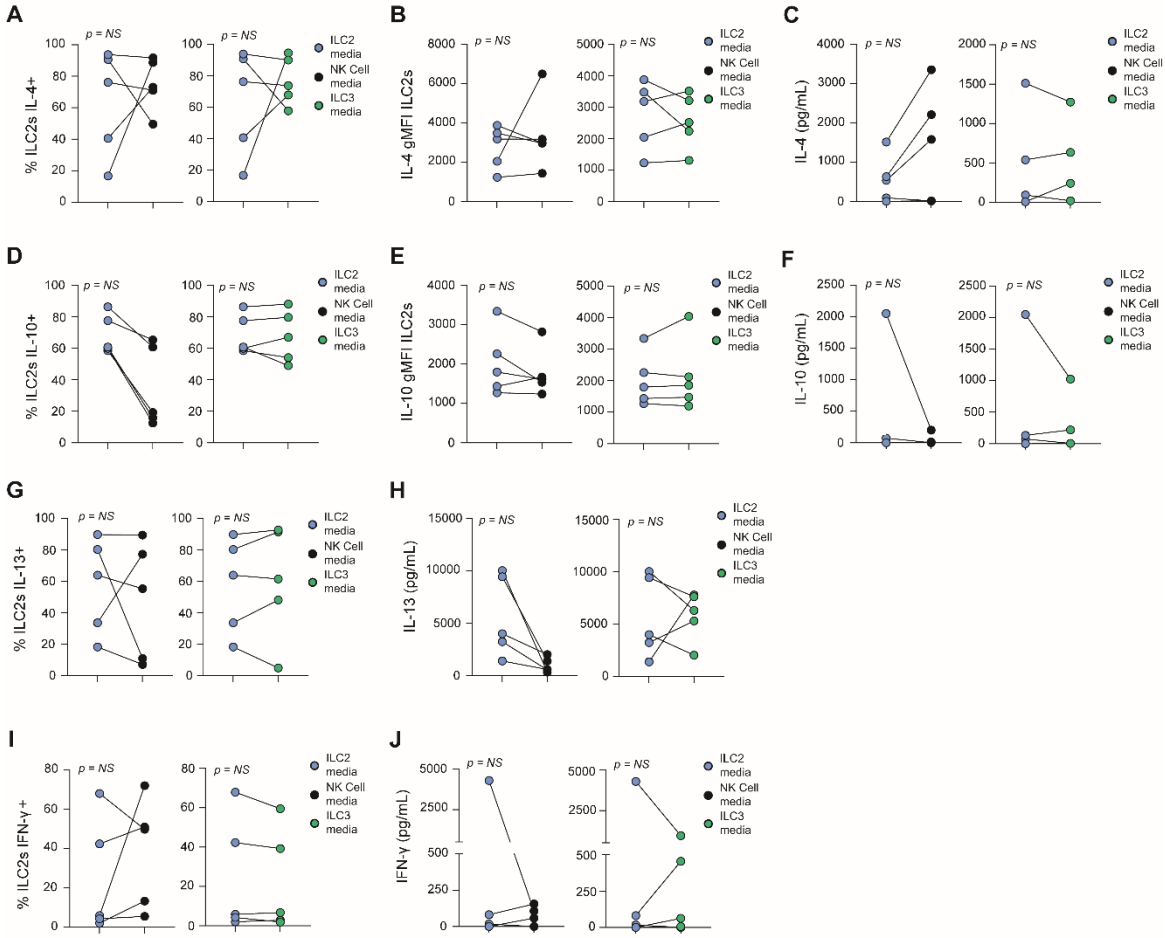

Supplemental Figure 3. Stability of signature cytokines on ILC2s with ILC2$_{10}$ phenotype upon culture in different cytokine conditions. ILC2$_{10}$ were expanded in ILC2 medium (X-VIVO15 Complete with IL-2, IL-7, and IL-33). These ILC2$_{10}$ were then removed from culture, washed, and plated in NK cell media (NK MACS medium with IL-2, IL-15, and IL-18) or ILC3 medium (X-VIVO15 Complete with IL-2, IL-7, IL-1β and IL-23). Intracellular cytokines were measured after 6-hour stimulation with phorbol 12-myristate 13-acetate and ionomycin and blocked with monensin and brefeldin A. **A,B** Expression of IL-4 on expanded ILC2$_{10}$ cultured in NK cell medium or ILC3 medium compared to ILC2 medium. This was measured as the percent of ILC2$_{10}$ positive for IL-4 (**A**) or the gMFI of IL-4 (**B**). (**C**) Cytometric bead array (CBA) analysis of changes in secreted IL-4 from ILC2s cultured in NK cell or ILC3 medium. **D,E** Expression of IL-10 on expanded ILC2$_{10}$ cultured in NK cell or ILC3 medium compared to ILC2 medium measured as the percent of ILC2s positive (**D**) or gMFI (**E**) of IL-10. (**F**) CBA analysis of changes in secreted IL-10 on expanded ILC2s subsequently cultured in NK cell or ILC3 medium. **G,H** Expression of IL-13 on expanded ILC2$_{10}$ cultured in NK cell or ILC3 medium compared to ILC2 medium measured as the percent of ILC2s positive (**G**) or gMFI (**H**) of IL-10. (**I**) Expression of IFN-γ on ILC2$_{10}$ cultured in ILC2 medium by percent positive following stimulation compared to culturing in NK cell or ILC3 medium. (**J**) CBA analysis of changes in secreted IFN-γ from ILC2s cultured in NK cell or ILC3 medium.

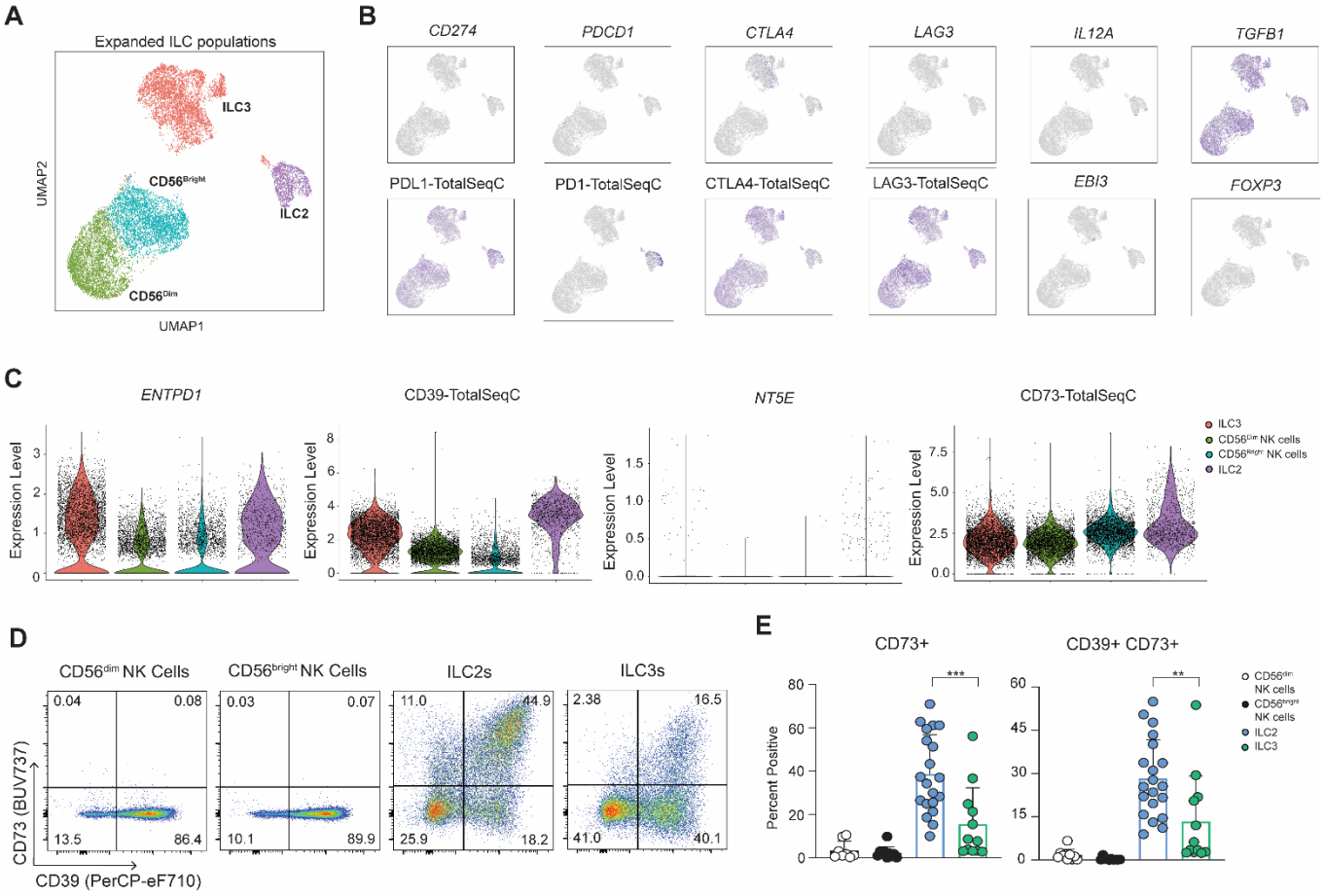

Supplemental Figure 4. Expression of nTreg and Tr1 markers on expanded ILC2s with ILC2$_{10}$ phenotype. (**A**) UMAP plots of expanded ILC subsets after CITE-seq. ILC subsets were isolated using FACS, expanded and then separately stained with an antibody cocktail. Each cell population was stained with a unique hashtag antibody to allow identification post sequencing. (**B**) Feature plots showing expression of markers linked to Treg and Tr1 cell function. Protein level expression is shown of PD-L1, PD-1, CTLA-4 and LAG-3 and RNA level expression of *CD274, PDCD1, CTLA4, LAG3, IL12A, EBI3, FOXP3* and *TGFB1* on expanded ILC subsets. (**C**) Violin plots of single cell expression of protein level CD39 and CD73 and RNA expression of *ENTPD1* and *NT5E* after expansion. Flow cytometry expression of CD39 and CD73 on expanded ILC subsets shown as representative flow plots (**D**) and summary graphs **(E)** (n = 10-20).

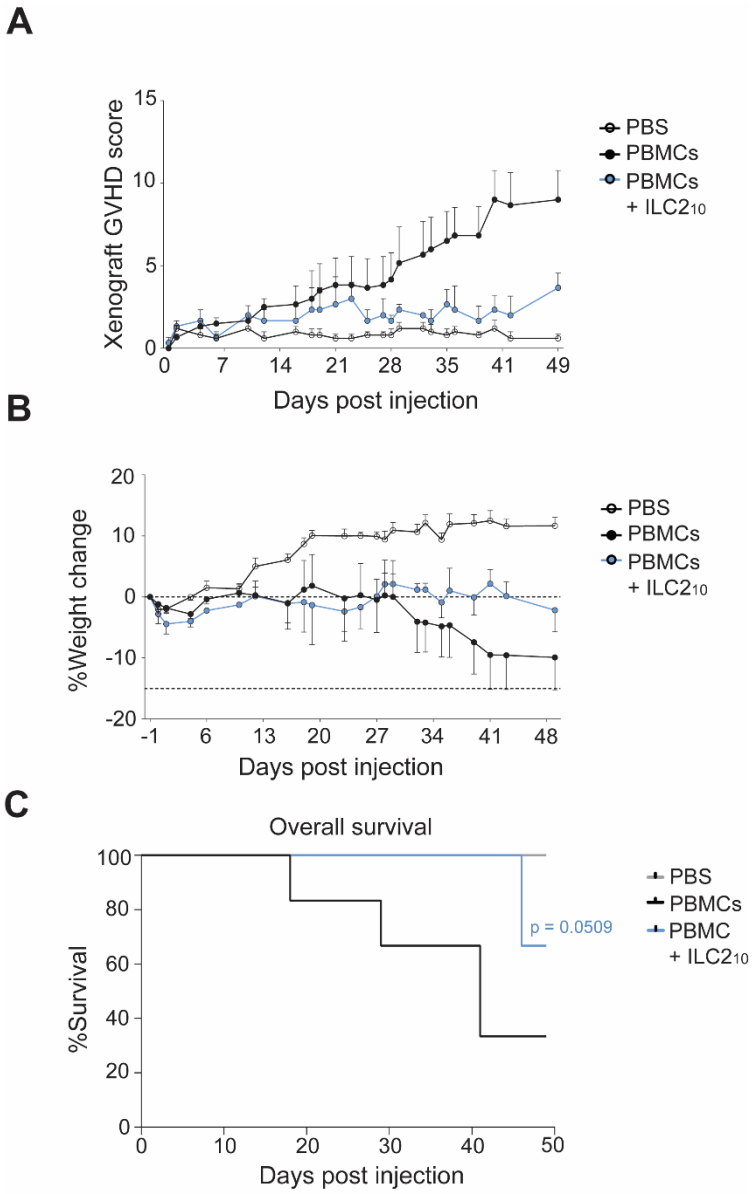

Supplemental Figure 5. Expanded human ILC2$_{10}$ suppress symptoms and improve survival of xenograft GVHD in male mice. (**A-C**) Xenogeneic GVHD score (**A**) weight loss (**B**) and overall survival **(C)** of male mice given PBS, 1x10^7 human PBMCs to induce xenograft GVHD or 1x10^7 PBMCs with an equal number of expanded human ILC2$_{10}$ over 7 weeks (n=5).

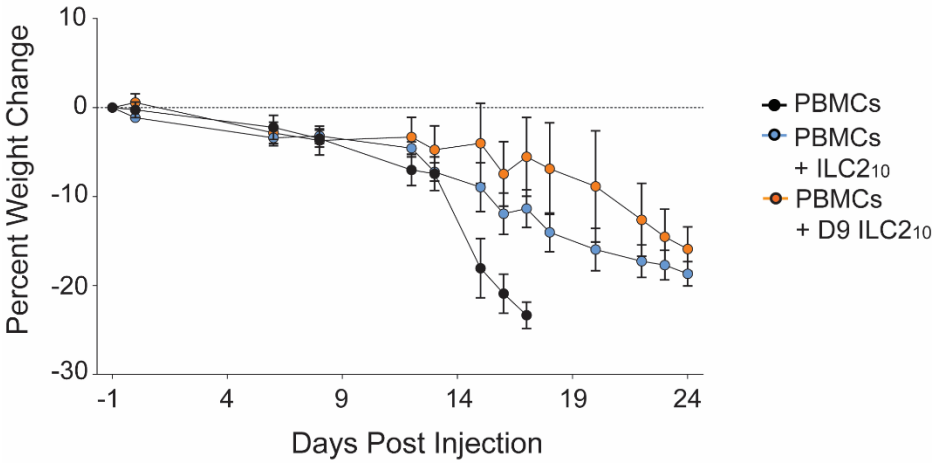

Supplemental Figure 6. Delayed injection of expanded human ILC2$_{10}$ improve weight-loss in xenoGVHD mice. Weight-loss over time of xenogeneic GVHD mice treated with expanded human allogeneic ILC2$_{10}$ at day 0 or 9 days following PBMC injection (n=3 for PBMC+ILC2$_{10}$ groups and n=5 for PBMCs alone).

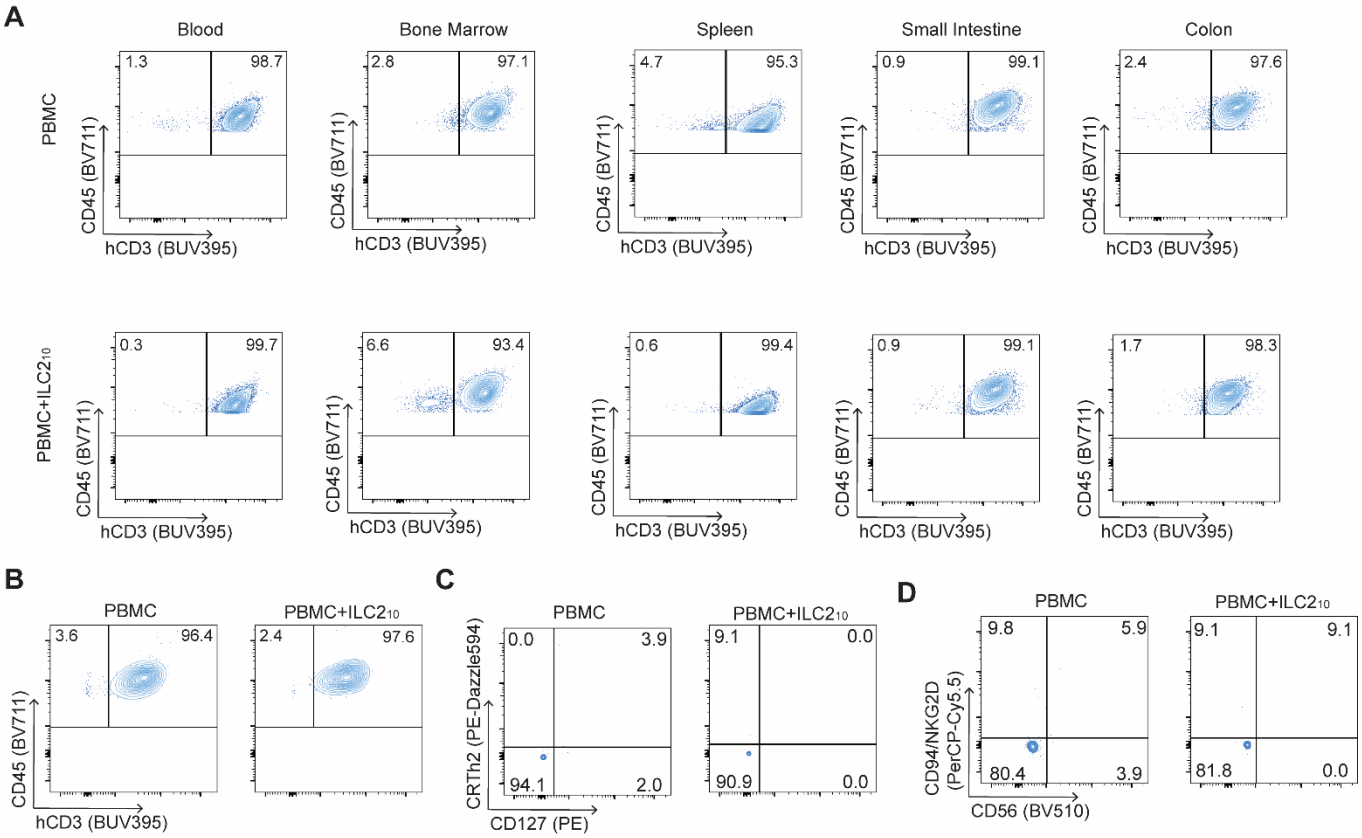

Supplemental Figure 7. Engrafted human CD45$^+$ cells are primarily T cells in xenogeneic GVHD mice. Flow cytometry plots of engrafted CD45$^+$ human cells in NSG mice given PBMCs alone or with allogeneic expanded ILC2$_{10}$. **A,B** Engraftment of human CD3$^+$ T cells gated on CD45$^+$ at endpoint (**A**) or day 14 post PBMC injection (**B**). **C,D** Proportion of human helper ILCs and ILC2s gated on CD45$^+$CD3$^-$ cells (**C**) and NK cells gated on CD45$^+$CD3$^-$ cells (**D**).

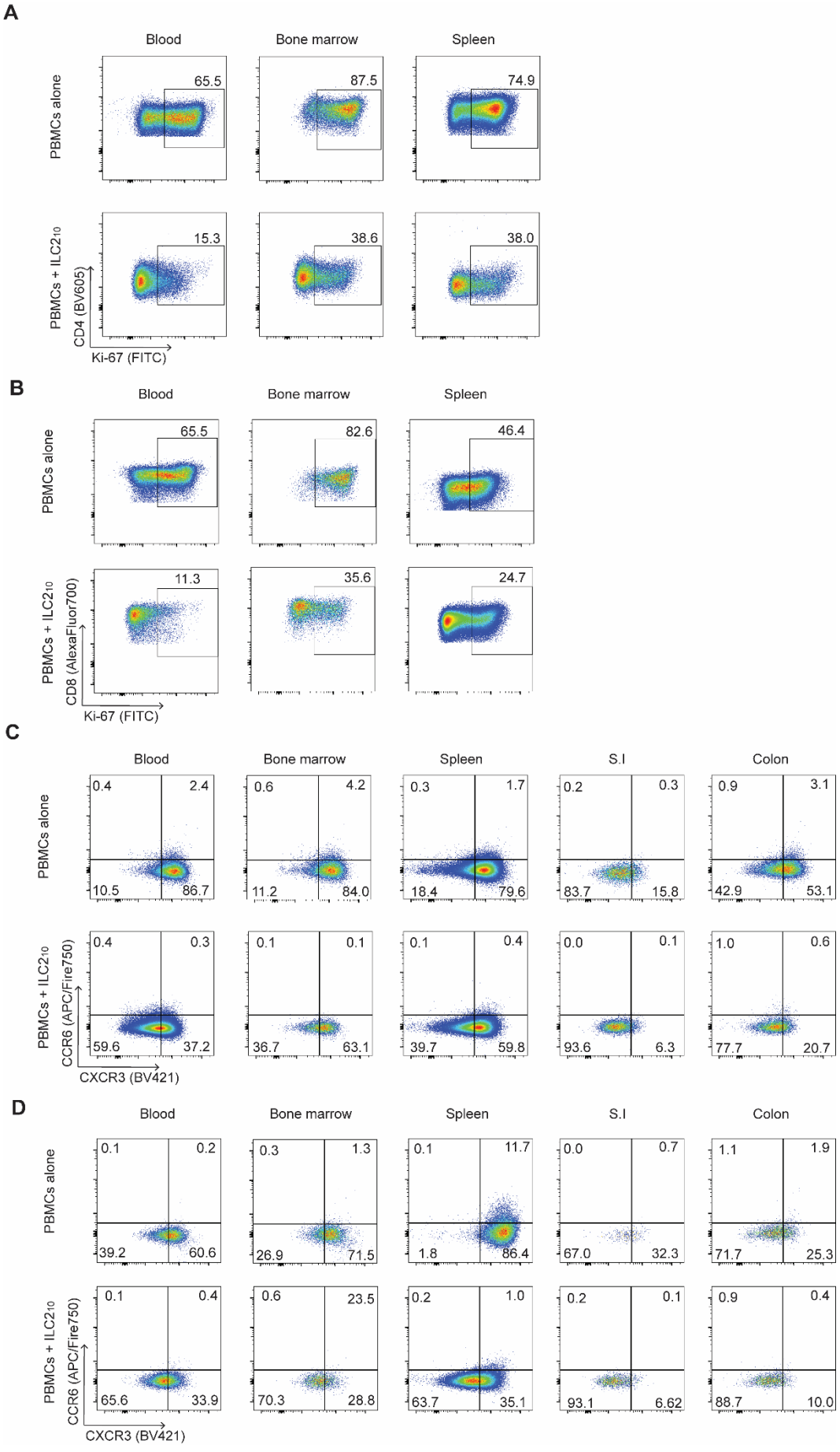

Supplemental Figure 8. Representative flow cytometry analysis of Ki-67 and CXCR3 on $CD4^+$ and $CD8^+$ T cells *in vivo* across tissues. A,B Representative FACS plots showing Ki-67 expression on $CD4^+$ (**A**) and $CD8^+$ (**B**) T cells in the blood, bone marrow and spleens of NSG mice given PBMCs or PBMCs with $ILC2_{10}$ infusion. **C,D** Representative FACS plots showing CXCR3 expression on $CD4^+$ (**C**) and $CD8^+$ (**D**) T cells in the blood, bone marrow, spleen, small intestines (S.I.) and colon of NSG mice given PBMCs or PBMCs with $ILC2_{10}$ infusion.

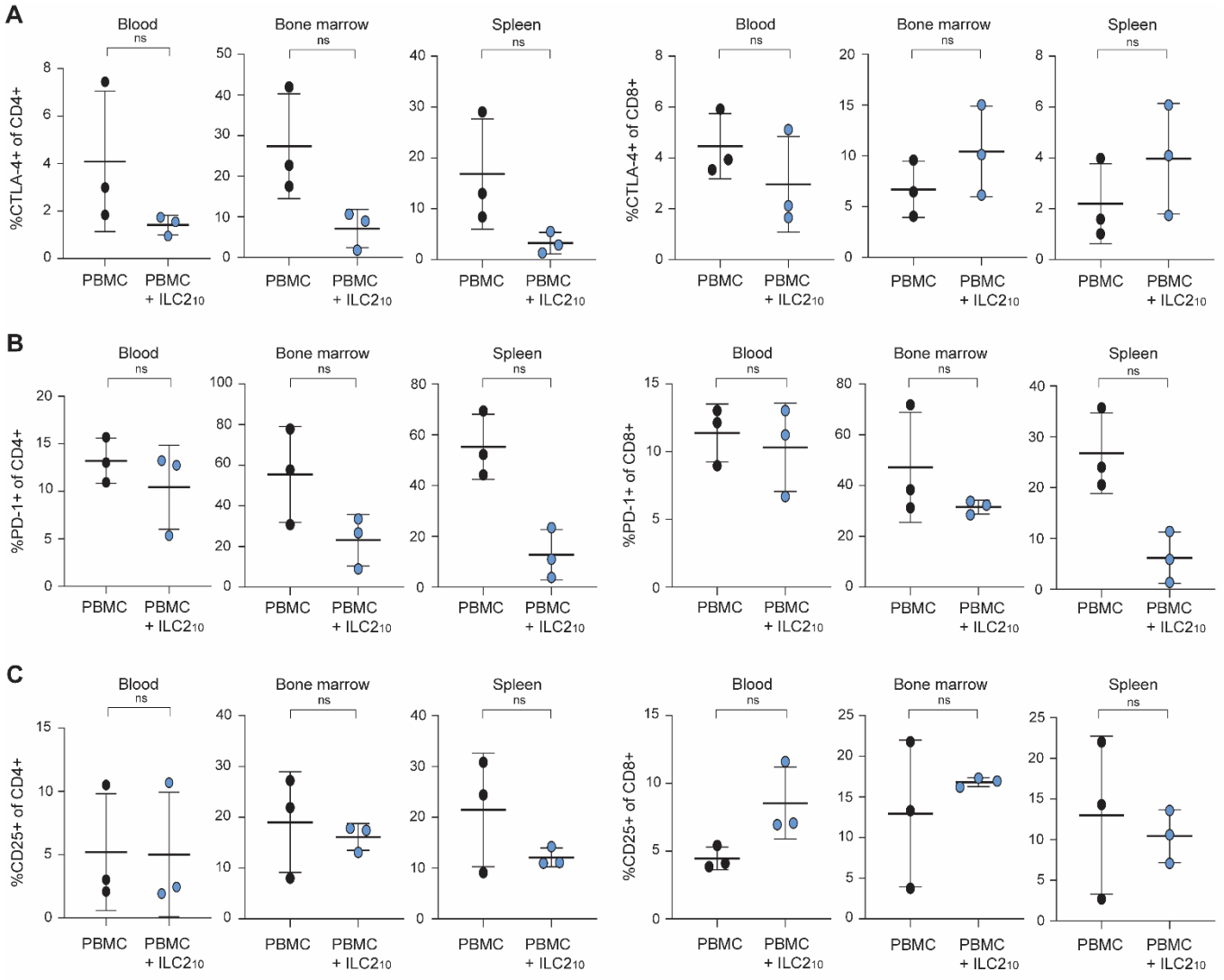

Supplemental Figure 9. Activation and checkpoint molecule expression on CD4$^+$ and CD8$^+$ T cells. **A-C** Expression of CTLA-4 (**A**) PD-1 (**B**) and CD25 (**C**) on CD4$^+$ and CD8$^+$ T cells in the blood, bone marrow and spleens of NSG mice given PBMCs or PBMCs with ILC2$_{10}$ infusion (n = 3).

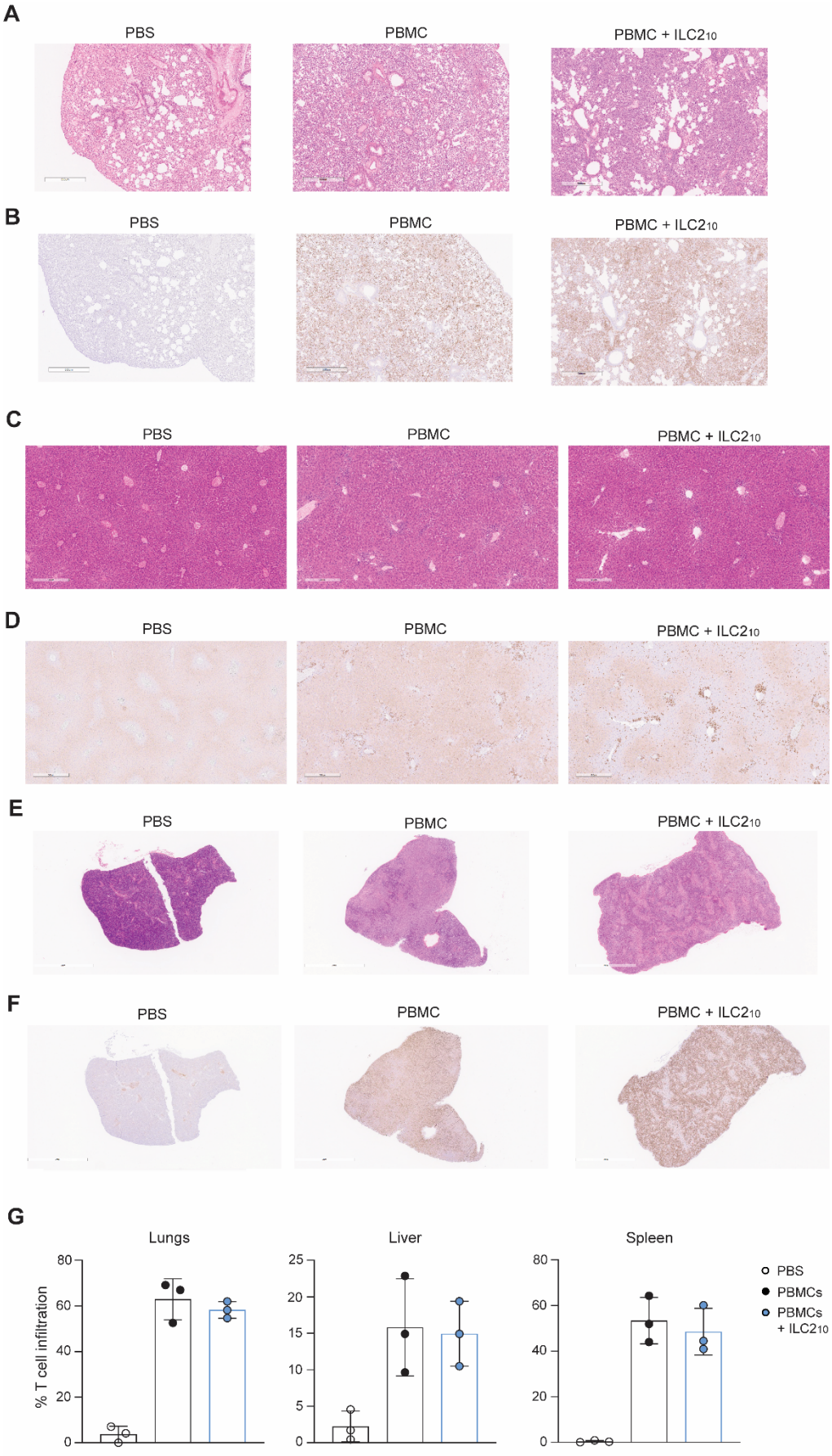

Supplemental Figure 10. H&E Staining and human CD3 immunohistochemical staining tissues of xenoGVHD mouse model. A,B Representative H&E (**A**) and human CD3 (**B**) staining on lungs from NSG mice given PBS, PBMCs or PBMCs with $ILC2_{10}$ taken at endpoint 8x magnification. **C,D** Representative H&E (**C**) and human CD3 (**D**) staining on livers from NSG mice given PBS, PBMCs or PBMCs with $ILC2_{10}$ taken at endpoint at 8x magnification. **E,F** Representative H&E (**E**) and human CD3 (**F**) staining on spleens from NSG mice given PBS, PBMCs or PBMCs with $ILC2_{10}$ taken at endpoint 2x magnification. (**G**) Average T cell infiltration in the lungs, liver and spleen of mice treated with PBS, PBMCs or PBMCs + $ILC2_{10}$. Quantified using CD3 immunohistochemistry and the HALO algorithm (n=3).

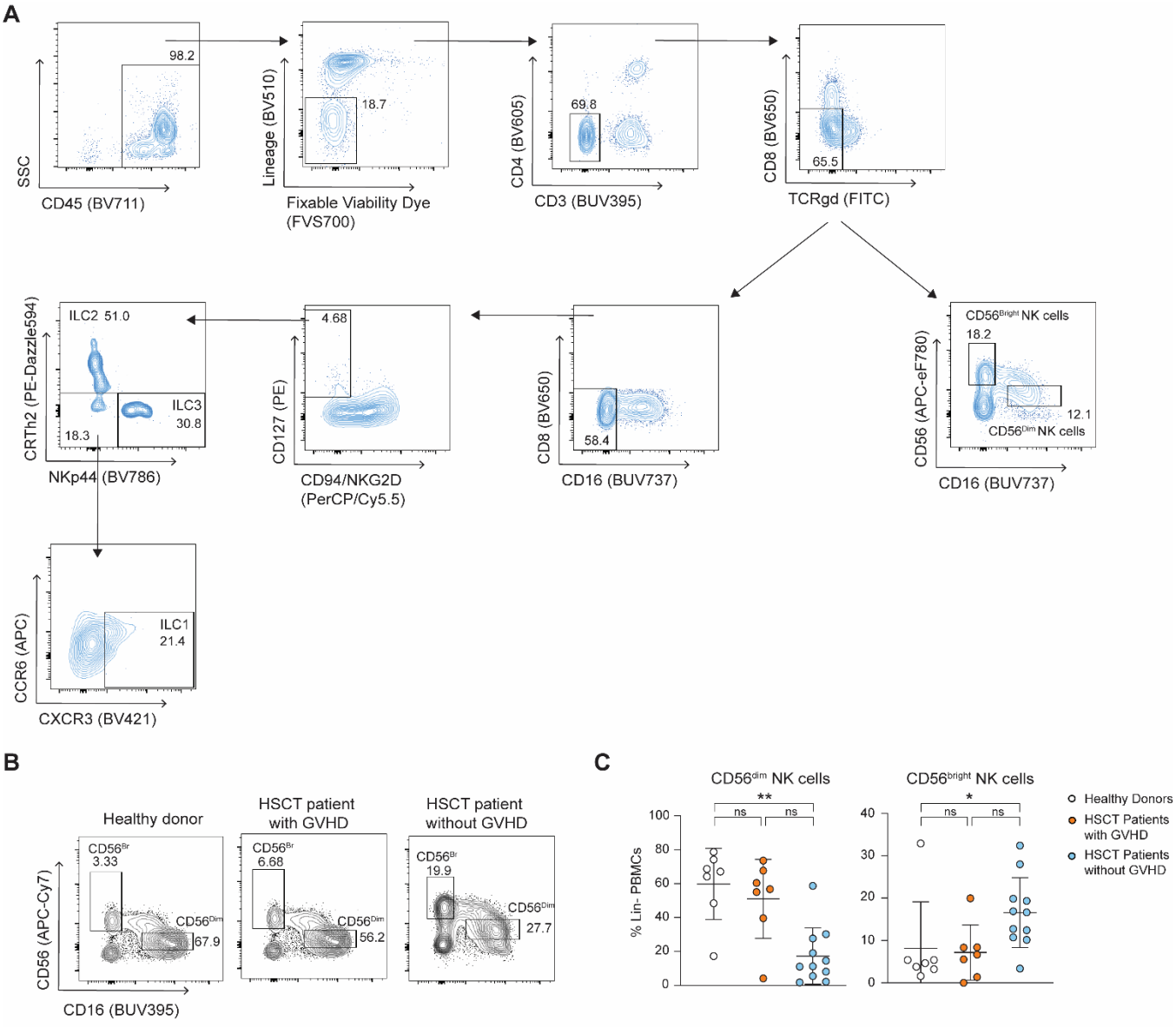

Supplemental Figure 11. ILC Gating strategy to analyze ILCs in HSCT recipient peripheral blood. PBMCs from healthy donors, and HSCT patients with or without aGVHD were assessed for ILC proportions and phenotypes using flow cytometry. (**A**) Lineage markers are CD14, CD19, CD20, CD33, CD34, CD123, CD138, CD303, and FCεRI. Cells are gated as $CD45^+$, $Lineage^-$, Live, $CD4^-$, $CD3^-$, $CD8^-$, and $TCR\gamma\delta^-$. NK cells are then gating as $CD56^+$ $CD16^+$ for $CD56^{dim}$ NK cells and $CD56^{bright}$ $CD16^-$ for $CD56^{bright}$ NK cells. Helper ILCs are then gated as $CD16^-CD94^-NKG2D^-CD127^+$ with ILC1s gated as $CD117^-CRTh2^-CXCR3^+$, ILC2s as $CRTh2^+$ and ILC3s as $CRTh2^-CD117^+$. **B,C** Representative flow plots (**B**) and summary graphs (**C**) of $CD56^{dim}$ $CD16^+$ and $CD56^{bright}$ $CD16^-$ NK cells in PBMCs, as a proportion of live $CD45^+$ lineage negative cells.

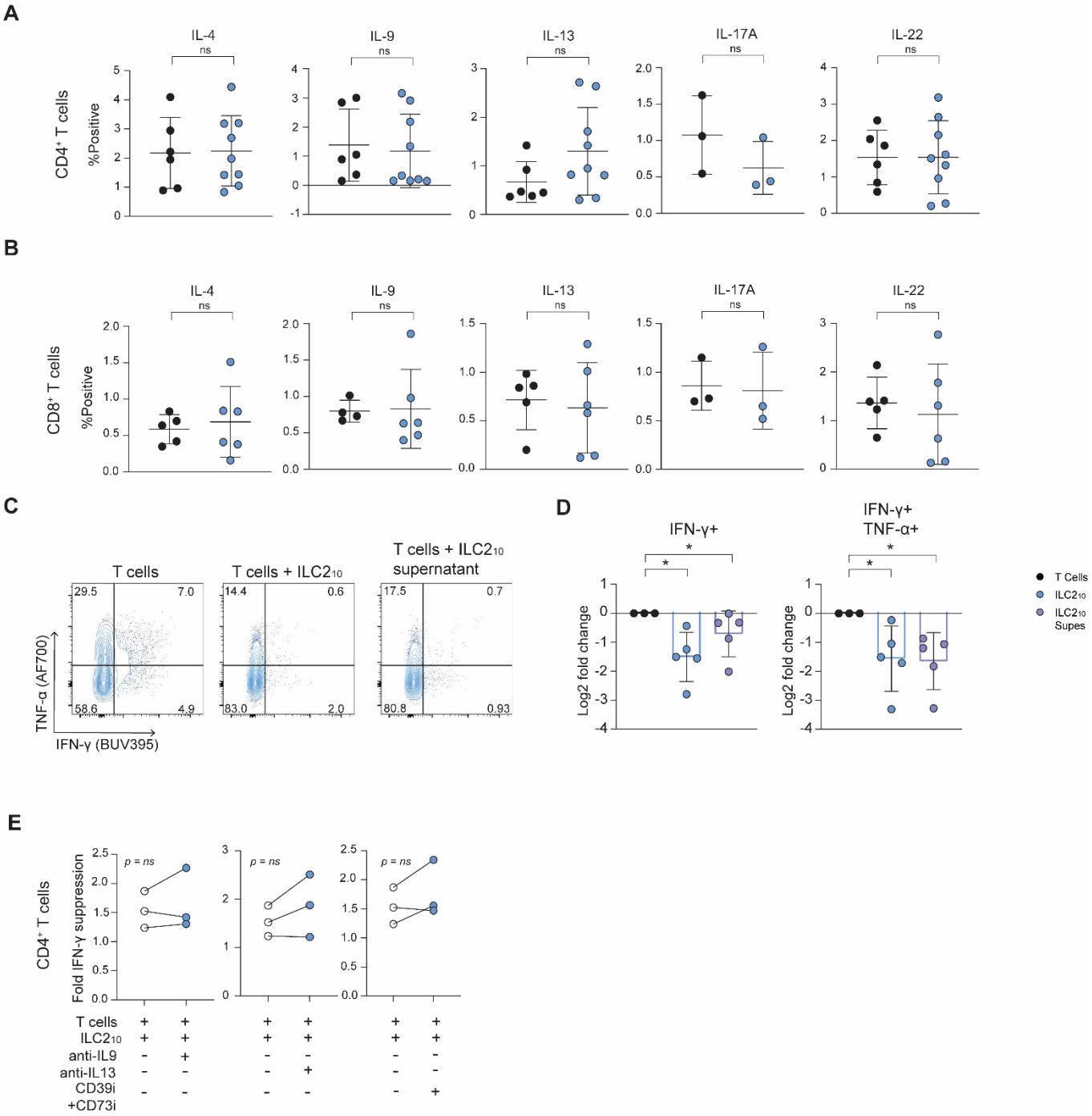

Supplemental Figure 12. Effect of $ILC2_{10}$ supernatant and addition of various inhibitors to $ILC2_{10}$-T cell co-cultures. A,B Summary graphs of intracellular IL-4, IL-9, IL-13, IL-17A and IL-22 on $CD4^+$ (n=6 T cells, n=9 $ILC2_{10}$)(**A**) and $CD8^+$ (n=5 T cells, n=6 $ILC2_{10}$) (**B**) T cells after co-culture with $ILC2_{10}$. **c,d** Representative FACS plots (**C**) and summary graphs (**D**) of IFN-γ expression by $CD4^+$ T cells cultured alone, with $ILC2_{10}$ or with $ILC2_{10}$ supernatant (n=5). (**E**) Changes in fold IFN-γ expression after co-culture of $CD4^+$ T cells with $ILC2_{10}$ with the addition of IL-9 or IL-13 antibodies or with CD39 and CD73 inhibitors on $CD4^+$ T cells (n=3).

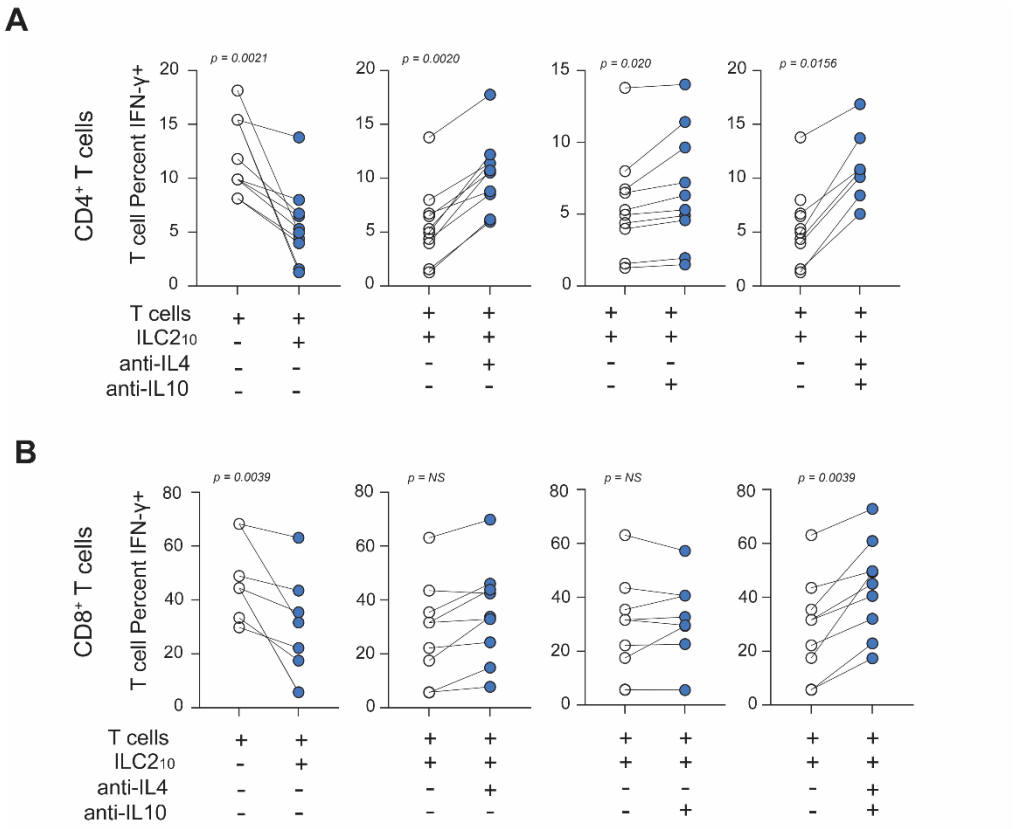

Supplemental Figure 13. Non-normalized IFN-γ expression on CD4$^+$ and CD8$^+$ T cells cultured with ILC2$_{10}$. (**A**) Percent expression of IFN-γ by CD4$^+$ T cells cultured alone or with ILC2$_{10}$ in the presence or absence of neutralizing antibodies towards IL-4, IL-10 and IL-4 and IL-10 together (n=10 from 5 independent experiments**) (B**) Percent expression of IFN-γ by CD8$^+$ T cells cultured alone or with ILC2$_{10}$ in the presence or absence of neutralizing antibodies towards IL-4, IL-10 and IL-4 and IL-10 together (n=7 from 5 independent experiments)

Supplemental Table 1: CITE-Seq TotalSeqC antibody details

Marker	Oligotag	Volume (µL per 1x10^6 cells)
CD56	TCCTTTCCTGATAGG	0.625
CD161	GTACGCAGTCCTTCT	1.04
CD117	AGACTAATAGCTGAC	2.5
CD16	AAGTTCACTCTTTGC	0.25
TIGIT	TTGCTTACCGCCAGA	5
CD335	ACAATTTGAACAGCG	1
CD294	TGTTTACGAGAGCCC	6.25
CD127	GTGTGTTGTCCTATG	0.5
CD196	GATCCCTTTGTCACT	0.125
CD314	CGTGTTTGTTCCTCA	2.66
CD336	GGGCAATTAGCGAGT	12.5
CD94	CTTTCCGGTCCTACA	0.5
KLRG1	GTAGTAGGCTAGACC	0.5
CD183	GCGATGGTAGATTAT	0.5
TCRγδ	CTTCCGATTCATTCA	1.0625
CD45	TCCCTTGCGATTTAC	0.4
TCRVα24-Jα18	AACTTCTGTGGTAGC	2.5
TCRαβ	CGTAACGTAGAGCGA	0.075
CD8a	GCTGCGCTTTCCATT	0.5
CD3	CTCATTGTAACTCCT	0.125
CD4	TGTTCCCGCTCAACT	0.25
CD138	ACTCTTTCGTTTACG	8.5
CD14	TCTCAGACCTCCGTA	0.125
CD206	TCAGAACGTCTAACT	1.67
HLADR	AATAGCGAGCAAGTA	2.65
CD45RO	TCAATCCTTCCGCTT	2.6
CD45RA	CTCCGAATCATGTTG	3.125
CD25	TTTGTCCTGTACGCC	0.5
CD223	CATTTGTCTGCCGGT	1.25
CX3CR1	AGTATCGTCTCTGGG	0.625
TLSPR	CAGTCCTCTCTGTCA	10
CD49b	GCTTTCTTCAGTATG	0.25
CD38	TGTACCCGCTTGTGA	0.5
CD57	AACTCCCTATGGAGG	0.125
CD49a	ACTGATGGACTCAGA	0.125
CD278	CGCGCACCCATTAAA	0.3125
CD357	ACCTTTCGACACTCG	5
CD39	TTACCTGGTATCCGT	0.25
CD69	GTCTCTTGGCTTAAA	0.625
CD279	ACAGCGCCGTATTTA	2.5

CD152	ATGGTTCACGTAATC	1.25
CD107a	CAGCCCACTGCAATA	0.15625
CD95	CCAGCTCATTAGAGC	1.25
CD134	AACCCACCGTTGTTA	0.625
CD137L	ATTCGCCTTACGCAA	1.25
CD40	CTCAGATGGAGTATG	0.025
CD137	CAGTAAGTTCGGGAC	10.625
CD194	AGCTTACCTGCACGA	2.125
CD27	GCACTCCTGCATGTA	0.425
CD28	TGAGAACGACCCTAA	0.03125
GARP	AGGTATGGTAGAGTA	2.5
CD122	TCATTTCCTCCGATT	2.5
CD184	TCAGGTCCTTTCAAC	2.5
CD49d	CCATTCAACTTCCGG	2.5
CD274	GTTGTCCGACAATAC	0.15625
CD120b	GCGCAACTCCTTGTA	0.255
CD80	ACGAATCAATCTGTG	0.625
CD32	GCTTCCGAATTACCG	0.10625
CD11b	GACAAGTGATCTGCA	0.2
CD64	AAGTATGCCCTACGA	0.10625
CD86	GTCTTTGTCAGTGCA	0.0425
CD163	GCTTCTCCTTCCTTA	0.53125
CD197	AGTTCAGTCAACCGA	0.5
CD73	CAGTTCCTCAGTTCG	10
Integrin β7	TCCTTGGATGTACCG	10
CD366	TGTCCTACCCAACTT	10
CD103	GACCTCATTGTGAAT	10

Supplemental Table 2: Patient and Healthy Donor Characteristics

		Acute GVHD (n=7)	No Acute GVHD (n=11)	Healthy Donors (n=7)
Sex M/F (%M)		5/2 (71.4)	6/5 (54.5)	4/3 (57.1)
Age				
	20-29	1 (14.3)	0 (0)	1 (14.3)
	30-39	0 (0)	2 (18.2)	0 (0)
	40-49	3 (42.9)	0 (0)	4 (57.1)
	50-59	0 (0)	4 (36.4)	1 (14.3)
	60-69	3 (42.9)	3 (27.3)	1 (14.3)
	70-79	0 (0)	2 (18.2)	0 (0)
Diagnosis				
	HL	1 (14.3)	0 (0)	N/A
	AML	3 (57.1)	7 (64.4)	N/A
	MF	0 (0)	1 (9.1)	N/A
	B-ALL	0 (0)	2 (18.2)	N/A
	MDS	3 (57.1)	1 (9.1)	N/A
Conditioning	RIC	5 (71.4)	6 (54.5)	N/A
	MAC	2 (28.6)	5 (45.5)	N/A
Donor	MUD	4 (57.1)	6 (54.5)	N/A
	MSD	2 (28.6)	3 (27.3)	N/A
	Haplo	1 (14.3)	2 (18.2)	N/A
Grade of aGVHD	1	1 (14.3)	0 (0)	N/A
	2	0 (0)	0 (0)	N/A
	3	4 (57.1)	0 (0)	N/A
	4	2 (28.6)	0 (0)	N/A
Immunosuppression	PTCγ	7 (100)	11 (100)	N/A
	CSA+Budesonide	2 (28.6)	0 (0)	N/A

Data expressed as n (%). HL, Hodgkin's Lymphoma; AML, acute myeloid leukemia; MF, myelofibrosis; BLL, B-cell acute lymphoblastic leukemia; MDS, myelodysplastic syndrome; RIC, reduced intensity conditioning; MAC, myeloablative conditioning; MUD, matched unrelated donor; MSD, matched sibling donor; Haplo, haploidentical transplant. PTCγ, post-transplant cyclophosphamide. CSA, cyclosporin.

Supplemental Table 3: Antibodies used for flow cytometry

Target	Fluorophore	Clone	Company	Dilution
Amphiregulin	PE	AREG559	eBioscience	1:25
CCR6	APC	G034e3	BioLegend	1:25
CCR6	APC/Fire750	G034e3	BioLegend	1:50
CD117	PE-Cy7	1D11	BioLegend	1:50
CD117	BV650	104D2	BioLegend	1:50
CD123	BV510	6H6	BioLegend	1:100
CD127	PE	HIL-7R-M21	BD	1:50
CD138	FITC	MI15	BioLegend	1:100
CD138	BV510	MI15	BioLegend	1:100
CD14	FITC	M5E2	BioLegend	1:200
CD14	BV510	M5E2	BioLegend	1:200
CD15	FITC	W6D3	BioLegend	1:200
CD16	PE-Dazzle594	3G8	BioLegend	1:100
CD16	BUV737	3G8	BD	1:100
CD19	FITC	HIB19	BioLegend	1:200
CD19	BV510	HIB19	BioLegend	1:200
CD20	FITC	2H7	BioLegend	1:200
CD20	BV510	2H7	BioLegend	1:200
CD203c	FITC	NP4D6	BioLegend	1:100
CD25	APC	BC86	eBioscience	1:25
CD3	FITC	OKT3	BioLegend	1:100
CD3	FITC	UCHT1	BioLegend	1:100
CD3	BUV395	UCHT1	BD	1:100
CD3	BUV496	SK7	BD	1:50
CD3	BV510	OKT3	BioLegend	1:100
CD303	BV510	201A	BioLegend	1:100
CD33	FITC	HIM3-4	BioLegend	1:100
CD33	BV510	P67.6	BioLegend	1:100
CD34	FITC	581	BioLegend	1:100
CD34	BV510	581	BioLegend	1:100
CD39	PerCP-eF710	eBioA1 (A1)	eBioscience	1:100
CD4	FITC	RPA-T4	BioLegend	1:200
CD4	BV605	RPA-T4	BD	1:200
CD45	BV711	HI30	BioLegend	1:100
CD45	BUV395	HI30	BD	1:100
CD49d	SuperBright600	9F10	eBioscience	1:50
CD56	BV605	HCD56	BioLegend	1:50
CD56	APC-Cy7	HCD56	BioLegend	1:50
CD73	BUV737	AD2	BD	1:50
CD79	FITC	HM47	BioLegend	1:100
CD8a	FITC	RPA-T8	BioLegend	1:200
CD8a	BV650	RPA-T8	BD	1:50
CD8a	AF700	RPA-T8	eBioscience	1:100

CD86	BUV737	2331 (FUN1)	BD	1:100
CD94	PerCP/Cy5.5	DX22	BioLegend	1:100
CRTh2	BV421	BM16	BioLegend	1:25
CRTh2	PE-Dazzle594	BM16	BioLegend	1:25
CTLA-4	PE-Cy7	14D3	eBioscience	1:50
CXCR3	BV421	G025H7	BioLegend	1:50
FCεR1a	FITC	AER-37	BioLegend	1:100
FCεR1a	BV510	AER-37	BioLegend	1:100
Fixable Viability Dye eF450	eF450	--	eBioscience	1:1000
Fixable Viability Dye eF506	eF506	--	eBioscience	1:1000
Fixable Viability Stain 700	FVS700	--	BD	1:1000
GM-CSF	APC	BVD2-21C11	BioLegend	1:50
IFN-γ	BUV395	B27	BD	1:100
IL-10	AF488	JES3-9D7	eBioscience	1:25
IL-10	PE	JES3-9D7	BioLegend	1:25
IL-13	BV711	JES10-5A2	BD	1:50
IL-17A	BV786	N49-653	BD	1:25
IL-17F	PE-CF594	033-782	BD	1:25
IL-22	eF450	22URTI	eBioscience	1:25
IL-4	PE-Cy7	MP4-25D2	BioLegend	1:100
IL-9	PerCP-eF710	MH9D1	eBioscience	1:50
Ki-67	FITC	20Raj1	eBioscience	1:25
KLRG1	BV786	2F1/KLRG1	BioLegend	1:50
NKG2D	PerCP/Cy5.5	1D11	BioLegend	1:100
NKp44	BV786	p44-8	BD	1:50
PD-1	BV785	EH12.2H7	BioLegend	1:100
TCRαβ	FITC	IP26	BioLegend	1:200
TCRγδ	FITC	B1	BioLegend	1:100
TNF-α	AF700	MAb11	eBioscience	1:50
Zombie NIR Fixable Viability Dye	Zombie NIR	--	BioLegend	1:1000

Supplemental Table 4: Lineage Antibodies for ILC Sort

Target	Fluorophore	Clone	Company	Dilution
CD138	FITC	MI15	BioLegend	1:100
CD14	FITC	M5E2	BioLegend	1:200
CD15	FITC	W6D3	BioLegend	1:200
CD19	FITC	HIB19	BioLegend	1:200
CD20	FITC	2H7	BioLegend	1:200
CD203c	FITC	NP4D6	BioLegend	1:100
CD3	FITC	OKT3	BioLegend	1:100
CD3	FITC	UCHT1	BioLegend	1:100
CD33	FITC	HIM3-4	BioLegend	1:100
CD34	FITC	581	BioLegend	1:100
CD4	FITC	RPA-T4	BioLegend	1:200
CD79	FITC	HM47	BioLegend	1:100
CD8a	FITC	RPA-T8	BioLegend	1:200
FCεR1a	FITC	AER-37	BioLegend	1:100
TCRαβ	FITC	IP26	BioLegend	1:200
TCRγδ	FITC	B1	BioLegend	1:100

Supplemental Table 5: Antibodies for ILC sort

Target	Fluorophore	Clone	Company	Dilution
CCR6	APC	G034e3	BioLegend	1:25
CD117	PE-Cy7	1D11	BioLegend	1:50
CD127	PE	HIL-7R-M21	BD	1:50
CD16	PE-Dazzle594	3G8	BioLegend	1:100
CD45	BV711	HI30	BioLegend	1:100
CD56	BV605	HCD56	BioLegend	1:50
CD94	PerCP/Cy5.5	DX22	BioLegend	1:100
CRTh2	BV421	BM16	BioLegend	1:25
Fixable Viability Stain 700	FVS700	--	BD	1:1000
NKG2D	PerCP/Cy5.5	1D11	BioLegend	1:100
NKp44	BV786	p44-8	BD	1:50

Supplemental Table 6: Intracellular Antibodies used for Flow Cytometry

Target	Fluorophore	Clone	Company	Dilution
Amphiregulin	PE	AREG559	eBioscience	1:25
GM-CSF	APC	BVD2-21C11	BioLegend	1:50
IFN-γ	BUV395	B27	BD	1:100
IL-10	AF488	JES3-9D7	eBioscience	1:25
IL-10	AF488	JES3-9D7	BioLegend	1:25
IL-10	PE	JES3-9D7	BioLegend	1:50
IL-13	BV711	JES10-5A2	BD	1:50
IL-17A	BV786	N49-653	BD	1:25
IL-17F	PE-CF594	033-782	BD	1:25
IL-22	eF450	22URTI	eBioscience	1:25
IL-4	PE-Cy7	MP4-25D2	BioLegend	1:100
IL-9	PerCP-eF710	MH9D1	eBioscience	1:50